Ore Geology Reviews 74 (2016) 196–210

Contents lists available at ScienceDirect

Ore Geology Reviews

journal homepage: www.elsevier.com/locate/oregeorev

Fluid inclusion geochemistry and Ar–Ar geochronology of the Cenozoic Bangbu orogenic gold deposit, southern Tibet, China

Xiaoming Sun [a,b,c,d,*], Huixiao Wei [a], Wei Zhai [b,c,**], Guiyong Shi [b,c,d], Yeheng Liang [b,c,d], Ruwei Mo [a], Moxiang Han [a,b], Jianzhou Yi [e], Xiangguo Zhang [e]

[a] School of Earth Science and Geological Engineering, Sun Yat-sen University, Guangzhou 510275, China
[b] School of Marine Sciences, Sun Yat-sen University, Guangzhou 510006, China
[c] Guangdong Provincial Key Laboratory of Marine Resources and Coastal Engineering, Guangzhou 510006, China
[d] South China Sea Bio-Resource Exploitation and Utilization Collaborative Innovation Center, Guangzhou 510006, China
[e] Geological Survey of Tibet Bureau of Geology and Mineral Exploration and Development, Lhasa 851400, China

ARTICLE INFO

Article history:
Received 3 August 2013
Received in revised form 13 November 2015
Accepted 15 November 2015
Available online 30 November 2015

Keywords:
Fluid inclusions
Ar–Ar dating
Cenozoic orogenic gold deposit
Continental collision
Bangbu gold deposit
Tibet

ABSTRACT

Located along the southern part of the Yarlung Zangbo suture zone in southern Tibet, Bangbu is one of the largest gold deposits in Tibet. Auriferous sulfide-bearing quartz veins are controlled by second- or third-order brittle fractures associated with the regional Qusong–Cuogu–Zhemulang brittle-ductile shear zone. Fluid inclusion studies show that the auriferous quartz contains aqueous inclusions, two-phase and three-phase CO_2-bearing inclusions, and pure gaseous hydrocarbon inclusions. The CO_2-bearing inclusions have salinities of 2.2–9.5% $NaCl_{eq}$, and homogenization temperatures (Th) of 167–336 °C. The δD, $\delta^{18}O$, and $\delta^{13}C$ compositions of the Bangbu ore-forming fluids are −105.5 to −44.4‰, 4.7 to 9.0‰ and −5.1 to −2.2‰, respectively, indicating that the ore-forming fluid is mainly of metamorphic origin, with also a mantle-derived contribution. The $^3He/^4He$ ratio of the ore-forming fluids is 0.174 to 1.010 R_a, and $^{40}Ar/^{36}Ar$ ranges from 311.9 to 1724.9. Calculations indicate that the percentage of mantle-derived He in fluid inclusions from Bangbu is 2.7–16.7%. These geochemical features are similar to those of most orogenic gold deposits. Dating by $^{40}Ar/^{39}Ar$ of hydrothermal sericite collected from auriferous quartz veins at Bangbu yielded a plateau age of 44.8 ± 1.0 Ma, with normal and inverse isochronal ages of 43.6 ± 3.2 Ma and 44 ± 3 Ma, respectively. This indicates that the gold mineralization was contemporaneous with the main collisional stage between India and Eurasia along the Yarlung Zangbo suture, which resulted in the development of near-vertical lithospheric shear zones. A deep metamorphic fluid was channeled upward along the shear zone, mixing with a mantle fluid. The mixed fluids migrated into the brittle structures along the shear zone and precipitated gold, sulfides, and quartz because of declining temperature and pressure or fluid immiscibility. The Bangbu is a large-scale Cenozoic syn-collisional orogenic gold deposit

© 2015 Elsevier B.V. All rights reserved.

1. Introduction

Since Groves et al. (1998) and Goldfarb et al. (2001) formerly proposed the model of "orogenic type gold deposit", numerous papers on the geological and geochemical features and genesis of the orogenic gold deposits in various metamorphic terranes around the world have been published (Goldfarb et al., 2001, 2004, 2005; Groves et al., 1998, 2003; Bierlein et al., 2004). Some researchers, such as Groves et al. (1998) and Kerrich et al. (2000), argued that the orogenic gold deposits are mainly present in accretionary orogens, whereas collisional orogens, such as the Alpine–Himalayan orogen, are not as favorable for preservation of orogenic gold deposits. In recent years, however, some large orogenic gold deposits have been discovered in the Qinghai–Tibet Plateau and in the collisional Ailaoshan gold belt in Yunnan Province (Sun et al., 2006, 2007a, 2007b, 2009; Xiong et al., 2007a, 2007b; Shi et al., 2012), the Longmenshan–Jinpingshan gold belt in western Sichuan Province (Luo and Yu, 2001; Wang et al., 2001; Yan et al., 2002; Li et al., 2005), the Xiaoqinling–Xiongershan gold province in the Qinling orogen (Chen et al., 1998, 2008; Zhou et al., 2014, 2015), the Tanjianshan deposit in the eastern Kunlun orogen, the Sawayaerdun deposit in the southwestern Tianshan (Chen et al., 2012a, 2012b), and the Erqis gold belt in the southern Altay (Chen et al., 2001). In addition, orogenic gold and gold–antimony deposits, such as Mayum, Zhemulang, and Mazhala, were discovered in southern Tibet along the Yarlung Zangbo suture zone. Geological and geochemical features suggest that the deposits are typical Cenozoic orogenic gold deposits formed during the early stage of India–Eurasia continental collision (Jiang

* Correspondence to: X. Sun, School of Earth Science and Geological Engineering, Sun Yat-sen University, Guangzhou 510275, China.
** Corresponding author.

http://dx.doi.org/10.1016/j.oregeorev.2015.11.021
0169-1368/© 2015 Elsevier B.V. All rights reserved.

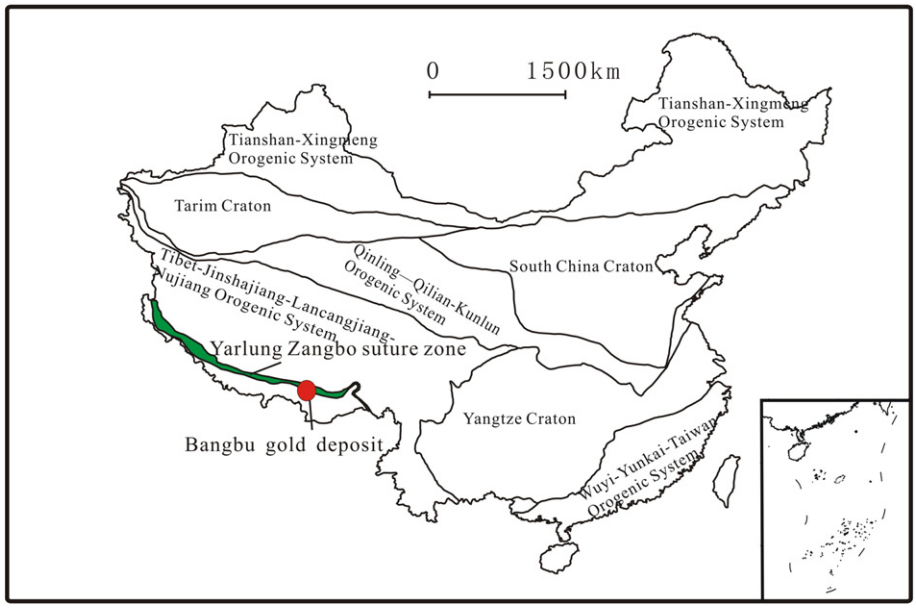

Fig. 1. Tectonic setting of Bangbu gold deposit (after Pan et al., 2009).

et al., 2008, 2009; Duoji and Wen, 2009; Zhai et al., 2014). Hence, the genesis and exploration potentials of orogenic-type gold deposits are now a very important issue to discuss.

Recently, a large gold deposit hosted in Late Triassic metamorphic rocks, Bangbu, was discovered in Jiacha County of southern Tibet. It is one of the largest lode gold deposits in Tibet and is located to the east part of the Yarlung Zangbo terrane suture zone. Preliminarily investigations have focused on the local geology and a tentative genetic model (Lu, 2005; Lv et al., 2005; Geological Survey of Tibet Bureau of Geology and Mineral Exploration and Development, 2006; Sun et al., 2010; Wei et al., 2010), and stressed that Bangbu may be an epithermal gold deposit. However, a systematic study of geochemical features and geochronology, critical for understanding the genesis, was lacking. In this study, microthermometric, Laser Raman, and stable isotope analyses of fluid inclusions, and Ar–Ar dating of hydrothermal sericite were performed on auriferous sulfide-bearing quartz veins from the Bangbu gold deposit. Our results suggest that it is a typical Cenozoic orogenic gold deposit formed during continental syn-collision.

2. Geological setting and geology of the Bangbu gold deposit

2.1. Regional geological setting

Tectonically, the Bangbu gold deposit is located on the southern side of the eastern Yarlung Zangbo suture zone in southern Tibet (Fig. 1), which marks the boundary between once widely separated continental masses of Eurasia and India (Allégre et al., 1984). The suture also marks the site where the Indus–Yarlung Zangbo Tethyan Ocean lithosphere

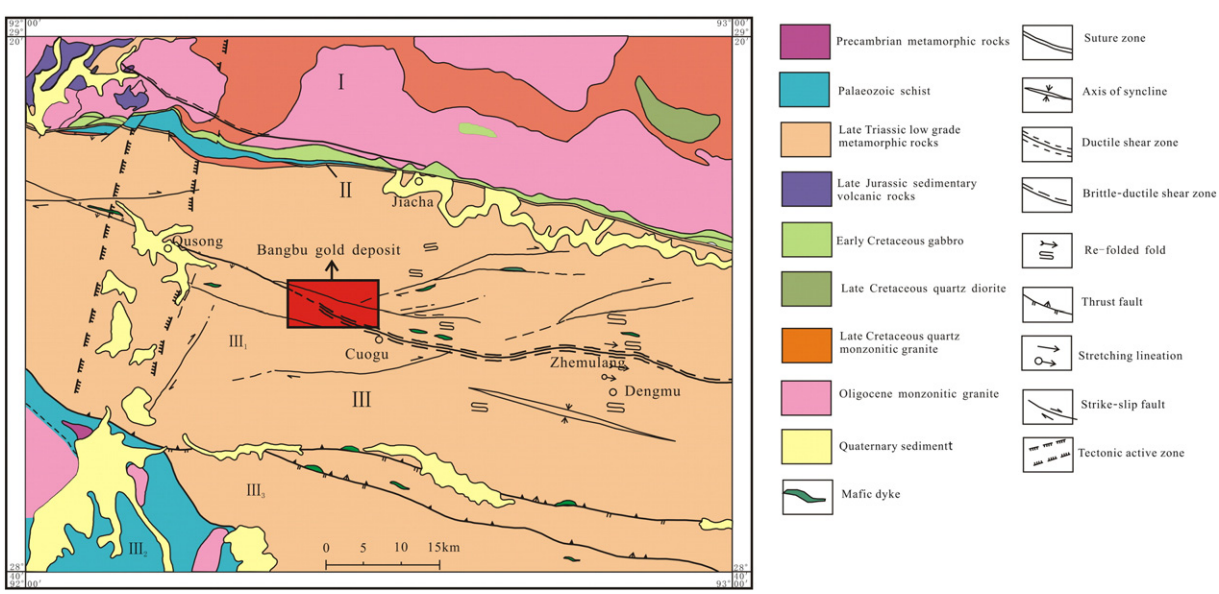

Fig. 2. Regional geological map of Bangbu gold deposit (modified after Geological Survey of Tibet Bureau of Geology and Mineral Exploration and Development, 2006). I — Gangdese block; II — Yarlung Zangbo tectonic suture zone; III — Himalayan block; III1 — Qusong–Dengmu slab; III2 — Qiongduojiang crystalline slab; III3 — Zongxu–Kala slab.

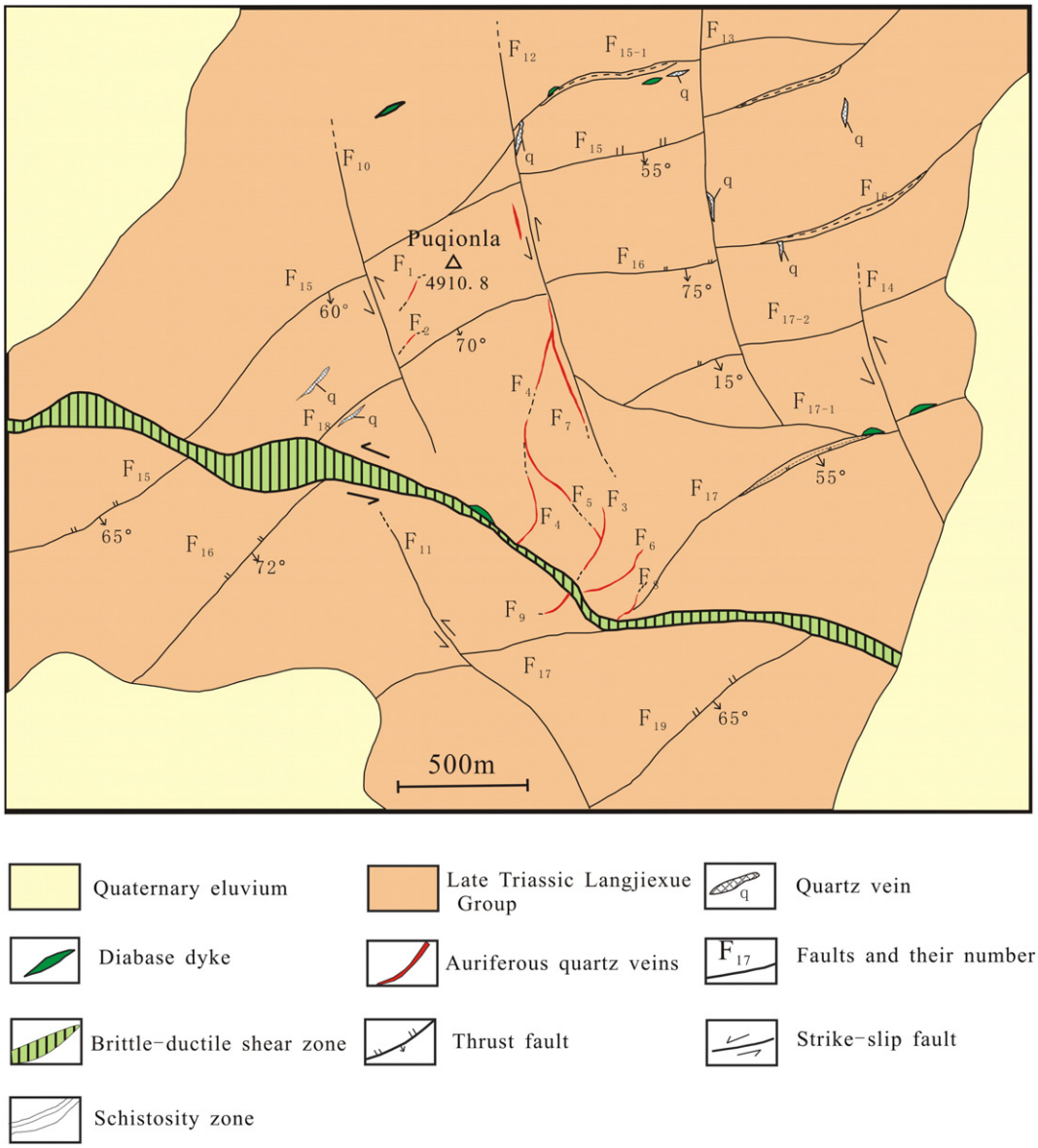

Fig. 3. Geological sketch map of Bangbu gold deposit (modified after Geological Survey of Tibet Bureau of Geology and Mineral Exploration and Development, 2006).

was consumed at a subduction zone dipping northward beneath the Lhasa terrane (Zhu et al., 2013). Investigations along the suture during the past decades have recognized several rock packages that represent fragments of ophiolites, generated in intra-oceanic island arc settings, together with their associated volcanic arc and subduction complexes (Aitchison et al., 2011; Zhu et al., 2013).

Table 1
Major features of main ore bodies in Bangbu gold deposit.

Number of ore body	General strike (°)	Length (m)	Occurrence		Average grade (10^{-6})	Ore types
			Direction of dip (°)	Dipping angle (°)		
I	10	>80			4.50	Native gold–limonite–pyrite brecciated quartz vein type
II-1	208	274	290–310	38	3.78	
II-2	49–346	340	210–330	34–39	3.71	Native gold–limonite–pyrite brecciated quartz vein type, Altered tectonite type
III	339	593	218–255	26–45	9.39	Native gold–limonite–pyrite brecciated quartz vein type
IV	30	108	110–120	29–32	3.27	
V	50	66	340	15	1.35	Native gold–limonite–pyrite brecciated quartz vein type, Altered tectonite type
VI	325	471	240–256	31–46	9.36	
VII	33	222	310–322	42–52	3.67	
VII	52	143	310–345	30–32	2.12	Native gold–limonite–pyrite quartz vein type
IX	66	373	320–340	30–33	5.54	
X	49	138	300–350	27–52	7.90	Native gold–limonite–pyrite brecciated quartz vein altered tectonite type

After Geological Survey of Tibet Bureau of Geology and Mineral Exploration and Development, 2006.

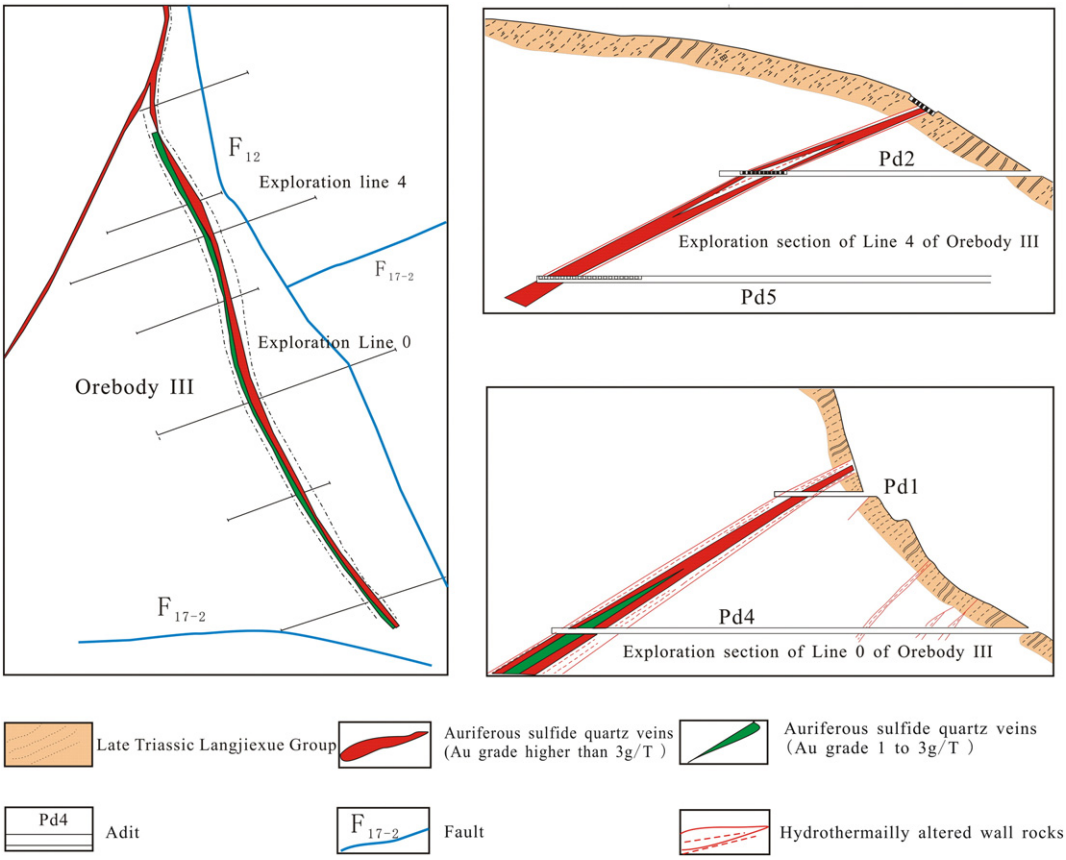

Fig. 4. Section sketch map of orebody III in Bangbu gold deposit (modified after Geological Survey of Tibet Bureau of Geology and Mineral Exploration and Development, 2006).

2.2. Geology of the Bangbu gold deposit

The Bangbu gold deposit is located near the center of the large-scale Qusong–Cuogu–Zhemulang brittle-ductile shear zone (Fig. 2). The shear zone is an E–W-striking sinistral fault, with a length of >40 km and a width of >1 km. Mafic dikes were emplaced along the shear, suggesting it is probably a very deep fault. Most of the orebodies in the Bangbu gold deposit are controlled by the NNW- and NE-striking second- to third-order brittle structures of the main shear zone (Fig. 3) (Geological Survey of Tibet Bureau of Geology and Mineral Exploration and Development, 2006; Lv et al., 2005).

The lithologies surrounding the gold deposit are mainly those of the Late Triassic Langjiexue Group, which includes marine argillites and greywackes that are mostly metamorphosed to lower greenschist facies. From oldest to youngest, the Langjiexue Group consists of the Jiedexiu, Jiangxiong, and Songre Formations. The Jiedexiu Formation is a carbonaceous and sericitic phyllite intercalated with feldspar–quartz siltstone. The Jiangxiong Formation consists of pyrite-bearing carbonaceous and sericitic phyllite intercalated with felsic sandstone and siltstone. The Songre Formation is composed mainly of carbonaceous and sericitic phyllite intercalated with felsic greywacke. The Bangbu gold deposit occurs predominantly in rocks of the Songre Formation. Most of the host rocks were strongly deformed and folded. Magmatic activity is limited in the deposit area, with only several small felsic and mafic dikes intruded along the faults in the region. The mafic dikes are distributed along the Qusong–Cuogu–Zhemulang brittle-ductile shear zone, are E–W-striking, and locally occur in swarms. The mafic dikes are typically tens of centimeters to tens of meters wide and tens to hundreds of meters long, and are locally regionally metamorphosed to chlorite–epidote–albite schists. The Au content in the mafic dikes can reach as high as 44 ppb, with an average content of 8 ppb Au, which is much higher than the regional background values of 1.5 ppb Au. Thus the dikes might have provided heat and ore-forming materials for the Bangbu gold deposit (Geological Survey of Tibet Bureau of Geology and Mineral Exploration and Development, 2006), although their age is still unknown.

The Bangbu deposit was discovered in 2003 by the Geological Survey of Tibet's Bureau of Geology and Mineral Exploration and Development during mineral prospecting. The Survey performed regional exploration in 2005 and detailed investigations in the area of the deposit in 2008. An ore processing plant was established in 2009. The reserves and average grade of the Bangbu deposit are >40 tonnes Au and 7 g/t Au, respectively. The mineralized area is 1600-m-long and 1500-m-wide, and outcrops between 4396 m and 4925 m elevation. The gold deposit consists of eight orebodies and three mineralized occurrences, which are distributed along NNW-striking (II-1, II-2, III, VI) and NE-striking faults (I, IV, V, VII, VIII, IX, X) (Fig. 3). Their major features are presented in Table 1. The orebodies and occurrences are composed mainly of auriferous sulfide-bearing quartz veins, as well as mineralized and altered wallrock.

Orebody III is the largest and is located in the center of the Bangbu gold deposit (Fig. 3). The auriferous veins in orebody III strike 218–255° and dip 26–45° to the southwest (Fig. 4). The orebody is 593 m in length and 25–158 m in width (Fig. 5), with an average grade of 9.39 g/t Au and a reserve of 16.06 tonnes.

Most of the ore at Bangbu is present as limonite-, pyrite-, and galena-bearing auriferous quartz veins (Fig. 6), with additional ore in pyrite-, galena-, sphalerite-, and chalcopyrite-bearing altered wallrocks. Gold occurs within quartz grains, adjacent to sulfide grains, and in fractures or as inclusions within the sulfides (Fig. 7). The diameter of the native gold grains is mainly 0.1–0.4 mm. The major gangue minerals include quartz, sericite, epidote, and carbonate. The major alteration associated

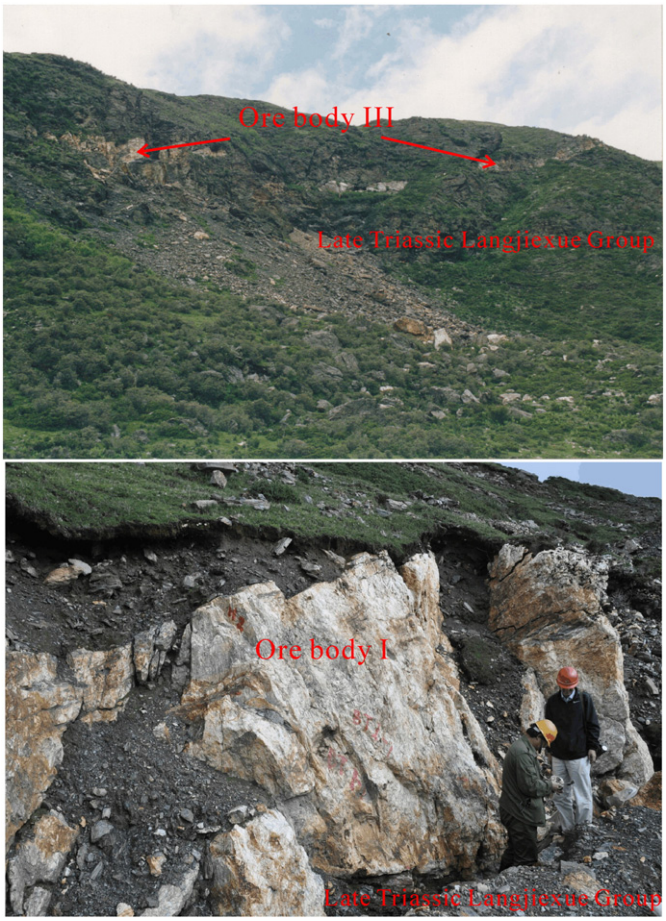

Fig. 5. Outcrops of auriferous sulfide quartz veins in Bangbu gold deposit. The upper photo is orebody III, the lower photo is orebody I. T_3S^{3-2}: Songre Formations of Late Triassic Langjiexue Group.

with the gold mineralization includes sulfidization, carbonatization, silicification, and sericitization.

3. Samples and analytical methods

Most of the samples used in this study were collected from orebody III, as well as from barren quartz veins adjacent to the mineralized area. The pyrite, quartz, and hydrothermal sericite selected for analyses were handpicked and examined carefully under the microscope.

The determination of inclusion paragenesis was according to the classification of primary, pseudosecondary, and secondary as outlined by Roedder (1984). The fluid inclusions in gold-bearing quartz and sphalerite are mainly primary and pseudosecondary, distributed as clusters, randomly, or in trails.

Fluid inclusion microthermometric measurements were performed using a Linkam THMSG600 heating/freezing stage in the School of Earth Sciences and Geological Engineering, Sun Yat-Sen University, Guangzhou. The analytical precision is 0.1 °C. Calibration was made using synthetic CO_2 fluid inclusions, pure-water inclusions, and potassium bichromate. The salinities and densities of inclusions were calculated using FLINCOR (Brown, 1989).

In-situ Laser Raman analyses for single fluid inclusions were carried out on a RENISHAW RM2000 Raman microspectrometer using 514.4 nm incident radiation produced by an argon laser in the Modern Analytical Center at Sun Yat-sen University and at the Guangzhou Institute of Geochemistry, Chinese Academy of Sciences. Analyses were performed at room temperature and a power of 5 mW. The detection limits are about 1 mol% for CO_2 and N_2.

Stable isotope analyses were performed in the Stable Isotope Laboratory of the Beijing Geological Research Institute of Nuclear Industry. The δD and $\delta^{13}C$ compositions of fluid inclusions in quartz were determined by thermal decrepitation to extract the fluid and carbonaceous material in fluid inclusions from ~5 g of sample consisting of mineral fragments that are 0.5 to 1.0 mm in diameter. The extracted water was reduced with carbon to generate H_2 and carbonaceous material was oxidized to CO_2 using Cu_2O at 650 °C for isotope analysis. For oxygen isotope analysis of the quartz, the samples were prepared by BrF_5 digestion (Clayton and Mayeda, 1963). The H, O, and C isotopic compositions were determined by using a MAT 251EM mass spectrometer. The standard is Standard Mean Ocean Water (SMOW) standard for H and O, and Pee Dee Belemnite (PDB) for C isotopic analysis. The analytical precision was 2‰ for δD, and 0.2‰ for $\delta^{18}O$ and $\delta^{13}C$. The $\delta^{18}O$ values of the hydrothermal quartz were calculated from fluid inclusion homogenization temperatures and the quartz–water oxygen isotope fractionation data of Clayton et al. (1972).

Noble gas isotopic analyses were performed at the National Key Laboratory of Gas Geochemistry, Lanzhou Institute of Geology, Chinese Academy of Sciences, using a Micromass MM5400 gas mass spectrometer. Analytical conditions were: $It_4 = 800$ Ma, $It_{40} = 200$ μa, 9.000 kV. All weighed samples of pyrite for analysis were packed into aluminum foil and shifted to a crucible for gas extraction under high vacuum conditions. When a pressure lower than 1×10^{-5} Pa was attained, the samples were heated at 130 °C for at least ten hours to eliminate secondary fluid inclusions and trace gases occurring along cleavage or in fractures. Then, the samples were fused at high temperatures of as much as 1000 °C, and the released gases were purified through the activated charcoal traps at the liquid nitrogen temperature to separate He from Ar. The minimum heat blanks for the MM5400 mass spectrum are: $^4He = 5.0 \times 10^{-12}$ cm^3 STP/g; $^{40}Ar = 9.0 \times 10^{-10}$ cm^3 STP/g. The standard for normalizing the analytical results is air in Lanzhou (AIRLZ2003); analytical precision for the noble gases isotopic measurements is better than 10% (Ye et al., 2001).

The Ar–Ar dating was carried out in the State Key Laboratory of Lithospheric Evolution, Institute of Geology and Geophysics, Chinese Academy of Sciences, Beijing, using the step-heating $^{40}Ar/^{39}Ar$ method. Samples of about 3 mg, together with multiple monitor samples of the 28.34 ± 0.28 Ma neutron fluence monitor mineral sanidine (85G003), were irradiated in a vacuum within a cadmium-coated quartz vial for 45.8 h in position H8 of the facility of Beijing Atomic Energy Research Institute reactor. Six to eight replicate analyses of the monitors from each position in the vials were conducted to constrain the vertical neutron fluence gradient to within ±0.7%. This additional uncertainty was propagated into the plateau and inverse isochron ages. Interfering nucleogenic reactions were checked for every irradiation by using CaF and K_2SO_4. Correction factors applied in this study are: $(^{36}Ar/^{37}Ar)_{Ca} = 2.609 \times 10^{-4} \pm 1.418 \times 10^{-5}$, $(^{39}Ar/^{37}Ar)_{Ca} = 7.236 \times 10^{-4} \pm 2.814 \times 10^{-5}$, $(^{40}Ar/^{39}Ar)_K = 2.648 \times 10^{-2} \pm 2.254 \times 10^{-4}$, $\lambda = 5.543 \times 10^{-10} a^{-1}$. Mass discrimination was monitored using an on-line air pipette from which multiple measurements are made before and after each incremental-heating experiment. The mean mass discrimination over this period is 1.00831 ± 0.00017 per amu and the uncertainty of this value is propagated into all age calculations. Isotopic measurements were made on a mass spectrometer MM5400 with a Faraday cup and an electron multiplier. The latter was used as the collector during this study. The detailed analytical methodology was described by Wang et al. (2006) and Chen et al. (2006).

4. Geochemistry of the ore-forming fluid

Microscope observations indicated numerous primary and pseudosecondary fluid inclusions in auriferous quartz and sphalerite from Bangbu, which were mostly 5–20 μm in diameter, and locally 50–60 μm. Most of the pseudosecondary inclusions were distributed

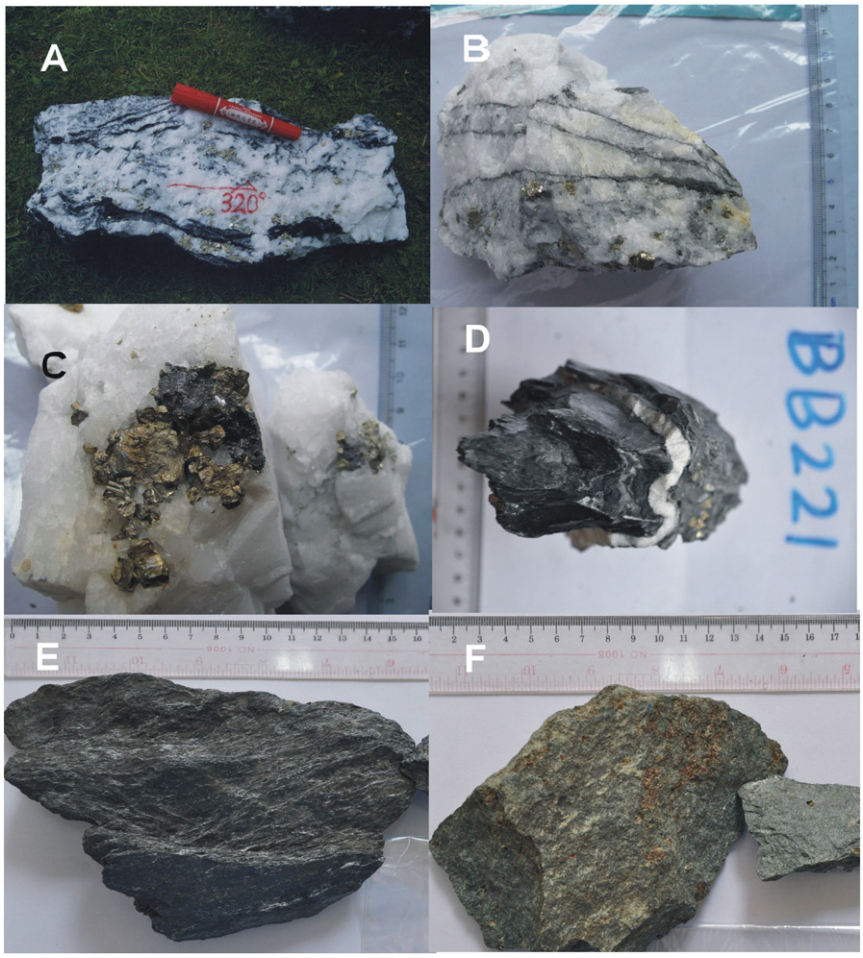

Fig. 6. Hand specimens of auriferous sulfide quartz veins and major host rocks in the Bangbu gold deposit. A—Auriferous sulfide quartz vein of orebody III, collected from gallery No.4; B—auriferous sulfide quartz vein (Sample No.2010069); C— auriferous sulfide quartz vein (Sample No.2010063); D—native gold in the auriferous quartz vein; E—hydrothermal sericite in auriferous quartz vein (Sample No.BB220); F—Upper Triassic carbonaceous sericite phyllite (Sample No.BB033); G—carbonaceous sericite mylonite hosting orebody III (Sample No.BB021); H—altered diabase collected from adjacent area of Bangbu gold district (Sample No.BB031).

in single quartz grains in a parallel and linear arrangement (Fig. 8A), and their microthermometric data are nearly the same as primary inclusions.

4.1. Types of fluid inclusions

Observations under the microscope, combined with microthermometric measurements and Laser Raman analyses, show that auriferous quartz veins contain three different types of fluid inclusions:

1. Liquid aqueous inclusions (type I), which are pure transparent liquid inclusions (Fig. 8B). There were no obvious changes in gas/liquid ratios during heating and cooling. Laser Raman analyses show that the major composition of type I fluid inclusions is H_2O (Fig. 9A, D).
2. CO_2-bearing inclusions (type II), which are the most important fluid inclusions in the Bangbu deposit. They can be subdivided into two-phase (type IIa) (Fig. 8B, C, B, E) and three-phase (type IIb) (Fig. 8B, C) inclusions. The CO_2 content in type IIa is low and can only recognized by Laser Raman analysis, which shows that the non-aqueous gas phase in type IIa also includes minor N_2 and CH_4, with the liquid phase composed of H_2O with only minor CO_2 (Fig. 9B, E). The type IIb is commonly three-phase at room temperature, consisting of L_{H2O}, L_{CO2} and V_{CO2}, from outside to inside in the fluid inclusions. The L_{H2O} is in different shades and generally transparent, whereas the L_{CO2} is usually dark-colored, within which the V_{CO2} occurs as constantly moving bubbles. The high and narrow peaks at 1285 cm^{-1} and 1388 cm^{-1} in the Laser Raman spectra of gaseous phases in type IIb (Fig. 9E) suggest that the CO_2 content in this type of fluid inclusion is quite high.
3. Pure gaseous hydrocarbon inclusions (type III), which are dark and single-phase inclusions at room temperature (Fig. 8D). No obvious changes were observed during heating and cooling. Laser Raman analyses indicate that type III fluid inclusions are composed of CH_4, C_2H_6, C_3H_8, and C_6H_6 (Fig. 9C, F).

Observations under the microscope also recognized necking-down of fluid inclusions (Fig. 8D), suggesting that some of the host quartz and sphalerite grains were locally deformed. In addition, coexistence of different types of fluid inclusions with very variable liquid/vapor ratios was recognized in the Bangbu samples, indicating fluid unmixing might have played an important role during gold mineralization (Roedder, 1984).

4.2. Microthermometry

In this study, the CO_2-bearing type II fluid inclusions were studied with a heating/cooling stage, and the results shown that the type IIa inclusions are in the H_2O–NaCl system, with ice melting temperatures of −2.4 to −6.2 °C and homogenization temperatures of 167–336 °C.

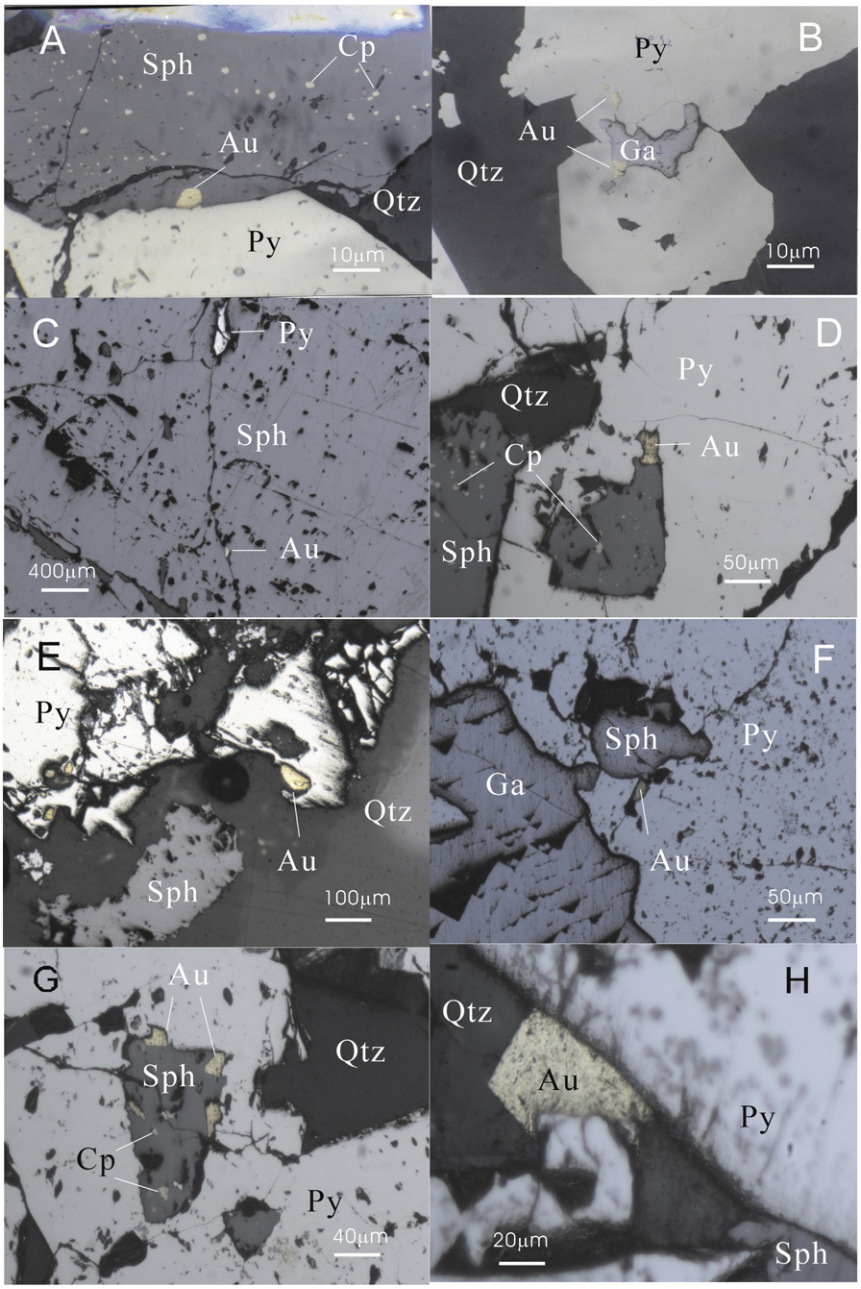

Fig. 7. Photomicrographs of native gold in auriferous sulfides quartz ores in Bangbu gold deposit. A—Native gold occurred between pyrite and sphalerite and emulsion texture of chalcopyrite in sphalerite; B—native gold and galena occurred in pyrites; C—native gold and pyrite fulfilled in fractures of sphalerite; D—native gold occurred between pyrite and sphalerite and emulsion texture of chalcopyrite in sphalerite; E—native gold occurred between pyrite and quartz; F—native gold occurred between pyrite, sphalerite and quartz; G—native gold occurred between pyrite and sphalerite and emulsion texture of chalcopyrite in sphalerite; H—native gold occurred between pyrite and quartz. Qtz: quartz; Au: native gold; Py: pyrite; Cp: chalcopyrite; Sph: sphalerite; Ga: galena.

The corresponding salinity is calculated as 3.9–9.5% $NaCl_{eq}$. The type IIb inclusions are in the CO_2–H_2O–NaCl system. Clathrate compounds were formed during cooling of the type IIb inclusions, and the melting temperature of the clathrates is 8.1–9.7 °C, and the partial homogenization temperature of CO_2 is 21.0–31.0 °C. Salinities calculated from the clathrate meltings are 2.2–3.7% $NaCl_{eq}$. The homogenization temperatures of type IIb inclusions are 264–307 °C.

The fluid inclusions in Bangbu, although with a broad range in fluid inclusion homogenization temperatures, have a distinct mode of 210–250 °C and an average of 235 °C (Fig. 10A). Salinities have a mode of 6.0–7.0 wt.% $NaCl_{eq}$ and an average of 6.25 wt.% $NaCl_{eq}$ (Fig. 10B), with density values of 0.63–0.96 g/cm^3, with a peak of 0.85–0.95 g/cm^3, and an average of 0.87 g/cm^3 (Fig. 10C). These data suggest that the ore-forming fluids at Bangbu are characterized by high CO_2, medium to low salinity, and moderate temperatures, which are similar to those of typical orogenic type gold deposits (Goldfarb et al., 2004; Groves et al., 1998.

4.3. Stable isotopes

The H–O–C isotope compositions of the ore-forming fluids at Bangbu are presented in Table 2. The results show that δD, $\delta^{18}O$, and $\delta^{13}C$ of the fluids are −105.5 to −44.4‰, 4.7 to 9.0‰, and −5.1 to −2.2‰, respectively. For comparison, a barren quartz vein (sample No.BB032) was

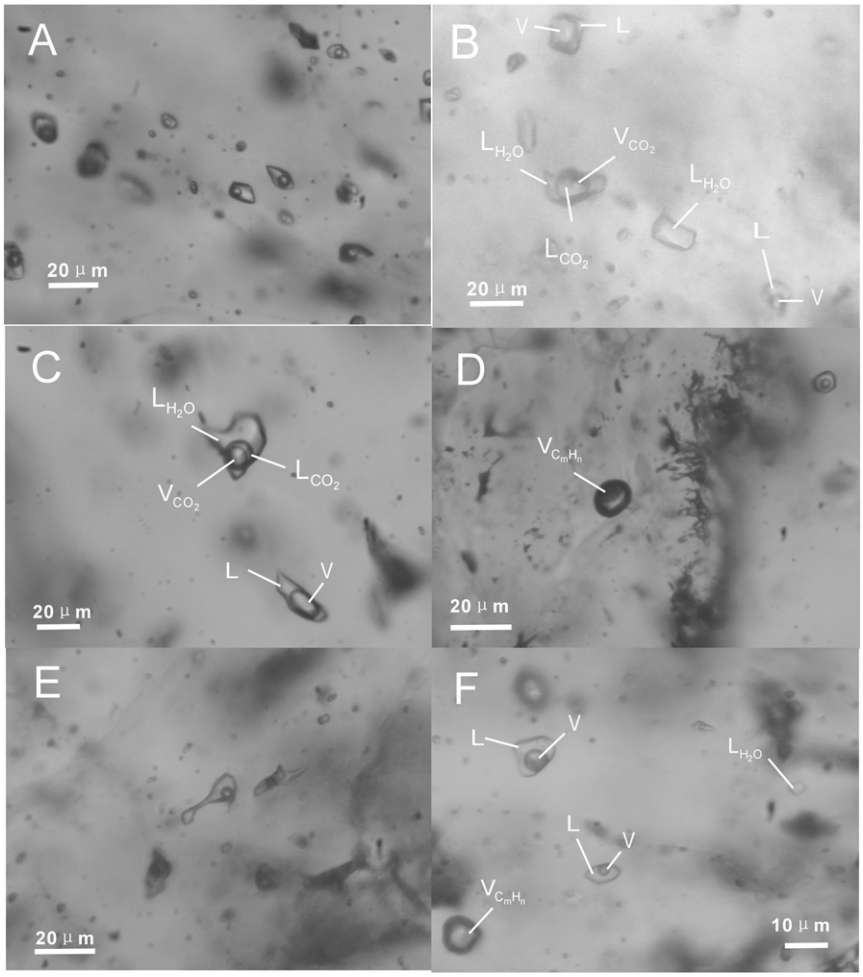

Fig. 8. Photomicrographs of fluid inclusions in quartz from the Bangbu gold deposit. A—Pseudosecondary fluid inclusions (sample BB003); B—coexistence of type I and II fluid inclusions with different liquid/vapor ratios (sample BB003); C—type IIa and IIb fluid inclusions (sample BB224); D—type III fluid inclusions (sample BB102); E—necking-down fluid inclusions (sample BB101); F—coexistence of three types fluid inclusions with different liquid/vapor ratios (sample BB104).

also analyzed, and its δD, $\delta^{18}O$, and $\delta^{13}C$ are −38.2‰, 6.1‰, and +5.1‰, respectively (Table 2).

4.4. Noble gas isotopes

The He–Ar isotope compositions of fluid inclusions in pyrite from the Bangbu auriferous veins and unmineralized host rock (sample No.BB017) were measured (Table 3). In the pyrite from the veins, ^4He values are(26.6–137.5) × 10^{-8} cm^3, averaging 62.9 × 10^{-8} cm^3; ^{40}Ar values are (8.01–237.0) × 10^{-8} cm^3, averaging 59.5 × 10^{-8} cm^3; R/R_a ratios are 0.174–1.010 (R is $^3He/^4He$ of sample, R_a is $^3He/^4He$ of air, and the value is 1.4 × 10^{-6}),averaging 0.58; and $^{40}Ar/^{36}Ar$ ratios are 311.9–1724.9, averaging 811.7. In contrast, the pyrite collected from unmineralized host rocks yielded a quite different noble gas isotopic composition, with ^4He of 901.0 × 10^{-8} cm^3, ^{40}Ar of 20.9 × 10^{-8} cm^3, R/R_a of 0.01137, and $^{40}Ar/^{36}Ar$ of 1709.7. In particular, the ^4He is much higher than that of the auriferous pyrites, whereas the R/R_a is much lower (Table 3).

5. Discussion

5.1. Source of ore-forming fluids

5.1.1. Stable isotope evidence

On a δD vs. $\delta^{18}O$ diagram (Fig. 11), most of the Bangbu samples plot within the fields of metamorphic and primary magmatic water, and are very close to the field of typical orogenic gold deposits (Goldfarb et al., 2004), and far from the meteoric water line, indicating that the ore-forming fluids are predominantly of metamorphic origin, with a small proportion of mantle-derived primary magmatic fluids. Carbon in hydrothermal fluids originates mainly from reservoirs that include the mantle with a $\delta^{13}C$ composition of −5.0 ‰ ± 2.0‰, sedimentary carbonate with an average $\delta^{13}C$ value of 0 ‰, and organic carbon with a $\delta^{13}C$ value typically of about −25 ‰ (Zheng and Chen, 2000). The $\delta^{13}C$ composition of CO_2 at Bangbu (−2.2 to −5.1‰) is similar to mantle-derived carbon, but He isotopes for fluid inclusions indicate that only small amounts of mantle He were present in the ore-forming fluid (see discussion below). Given that the proportion of mantle He and carbon in the ore fluid is the same, most of the carbon in ore fluid may have originated from orogenic and sedimentary carbon sources, which were devolatilized during regional metamorphism. The $\delta^{13}C$ values at Bangbu also lie in the range of granulite facies lower crust (−10‰ to −1‰, Moecher et al., 1994), implying that part of the CO_2 in the Bangbu may have come from the lower crust, which was probably a thickened juvenile mafic one developed during the collisional transpressional and extensional regime in southern Tibet (Hou et al., 2009, 2011).

5.1.2. Noble gas isotopic compositions

In recent years, He and Ar isotopic systematics have been used as source indicators for ore-forming fluids (Simmons et al., 1987;

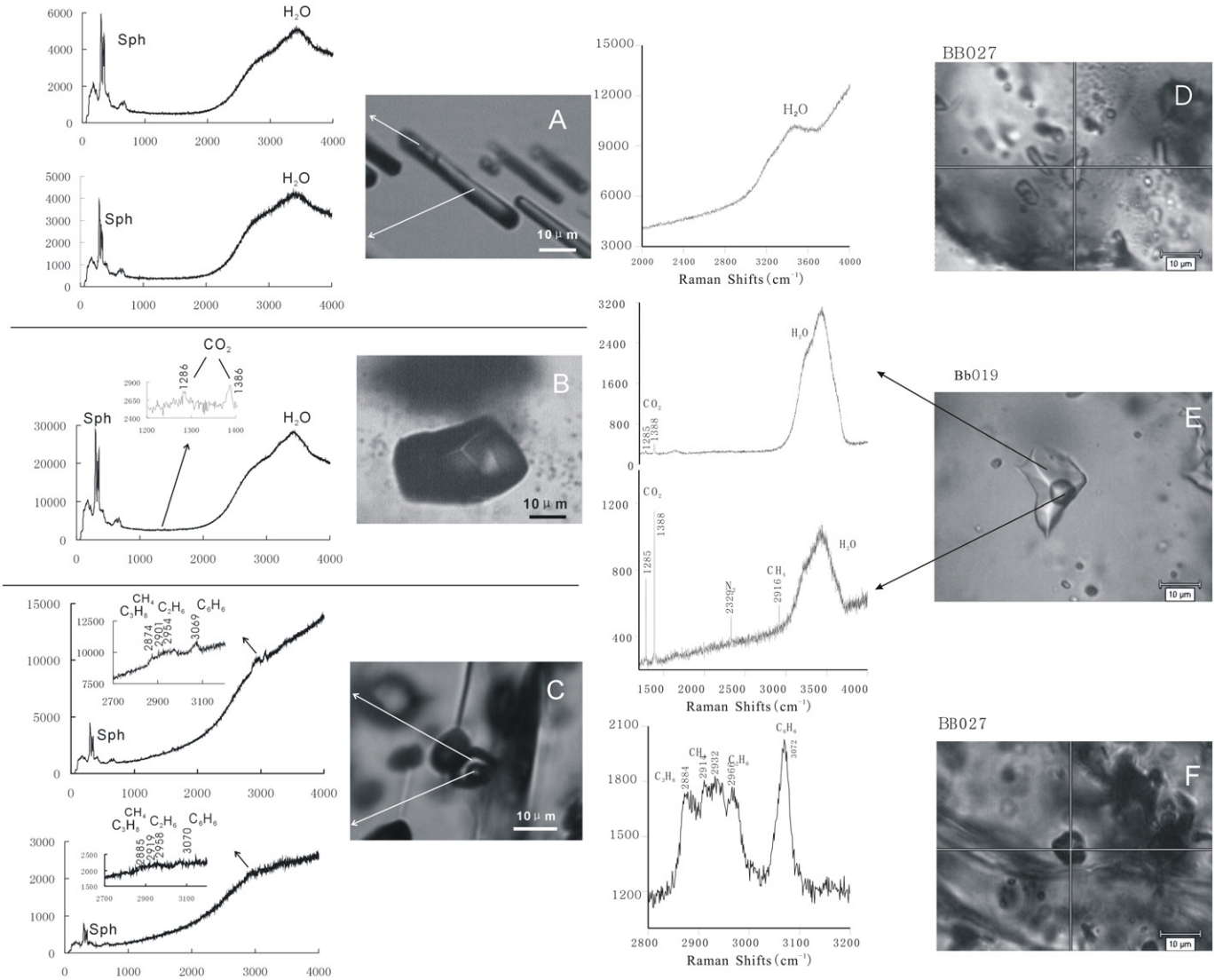

Fig. 9. Laser Raman analysis of fluid inclusions in sphalerite (A, B, C) and quartz (D, E, F) from Bangbu gold deposit. A. Laser Raman analyses indicate that the composition gaseous phases and liquid phases of type I fluid inclusions is H_2O (Sample 2,010,070); B. Laser Raman analyses indicate that type II fluid inclusions are composed of gas-phase CO_2 and H_2O (Sample 2,010,065); C. Laser Raman analyses indicate that the gaseous phases and liquid phases in type III fluid inclusions are C_mH_n (include CH_4, C_2H_6, C_3H_8 and C_6H_6) (Sample 2010070). D. Laser Raman analyses indicate that the composition of type I fluid inclusions is H_2O (Sample BB027). E. Laser Raman analyses indicate that the gaseous phases in type IIa fluid inclusions are composed predominantly of CO_2 and H_2O with a little N_2 and CH_4, and the liquid phases are composed of H_2O with a little CO_2 (Sample BB019). F. Laser Raman analyses indicate that type III fluid inclusions are composed of gas-phase C_mH_n (include CH_4, C_2H_6, C_3H_8 and C_6H_6) (Sample BB027).

Stuart et al., 1995; Hu et al., 1997; Sun et al., 1999, 2004, 2006, 2009; Burnard et al., 1999; Zhao et al., 2002; Winckler et al., 2001; Zeng et al., 2001; Mao et al., 2002, 2003; Ballentine et al., 2002; Xue et al., 2003). The major reasons for this include the fact that noble gas compositions are unaffected during water–rock interaction and the He–Ar isotopic compositions of various source reservoirs are quite different.

Noble gas isotopic compositions of fluid inclusions may be used as indicators of fluid sources (Burnard et al., 1999). Air-saturated water (ASW), including meteoric water and sea water, has $^3He/^4He$ and $^{40}Ar/^{36}Ar$ values of 1 R_a and 295.5 respectively. Mantle or deep-crustal magmatic water typically has $^3He/^4He$ and $^{40}Ar/^{36}Ar$ values that are 6–9 R_a and >40,000. Crustal fluids are characterized by $^3He/^4He$ and $^{40}Ar/^{36}Ar$ values of 0.01–0.05 R_a and >295.5.

Previous studies proved that noble gases such as He and Ar trapped in fluid inclusions in pyrites do not leak because of the lack of cleavage (Hu et al., 1997). Thus the He and Ar isotopic compositions may reflect He–Ar isotopic systematics of the ore-forming fluids for the Bangbu gold deposit.

Data for pyrite separates from the Bangbu veins are mainly scattered between ASW, mantle-derived (M), and crustal fluids (C) on Fig. 12. The fact that the Bangbu gold deposit is associated with a deep crustal shear zone, and the ore-forming fluid is predominantly a CO_2-bearing metamorphic fluid, is consistent with the noble gas data suggesting mainly crustal and mantle-derived fluids, with negligible ASW. Most of the Bangbu samples are scattered between crustal He and mantle-derived He on Fig. 13, also suggesting mantle-derived water might have been added to the ore-forming fluids at Bangbu.

The R/R_a of pyrite from unmineralized host rocks is very low (Table 2). It plots in the crustal fluid field on Figs. 12 and 13, indicating that this type of pyrite does not contain any mantle contribution. It is notable that all samples of this pyrite have a high content of $^4He(901 \times 10^{-8}$ cm^3 STP/g), suggesting that the pyrite might have been precipitated from metamorphic fluids, which are rich in ^4He and were probably generated during regional metamorphism of the country rocks.

On the assumption that the ore-forming fluids in Bangbu are composed mainly of crustal and mantle-derived waters, the percentage of

mantle-derived He may be estimated based on the following formula (Xu et al., 1996):

$$Mantle-derived-He(\%) = \frac{(^3He/^4He)_{Sample} - (^3He/^4He)_{Crust}}{(^3He/^4He)_{Mantle} - (^3He/^4He)_{Crust}} \times 100$$

The two end-member $^3He/^4He$ values for crustal and mantle fluids, 0.01 R_a and 6 R_a, are used in the calculation. The estimated percentage of mantle-derived He in auriferous pyrite is 2.7–16.7%, whereas no mantle contribution is present in pyrite from unmineralized host rocks (Table 3), suggesting that the mantle component was specifically involved in the gold mineralization process. Previous study of deposits in the Ailaoshan gold belt in Yunnan Province also demonstrated that mantle-crust interaction and addition of mantle-derived fluids played a key role during gold mineralization (Sun et al., 2006, 2009).

5.2. Age of the Bangbu mineralization

Dating by $^{40}Ar/^{39}Ar$ techniques was performed on hydrothermal sericite collected from auriferous quartz veins in the Bangbu deposit. Results yielded a plateau age of 44.8 ± 1.0 Ma, as well as normal and inverse isochronal ages of 43.6 ± 3.2 Ma and 44 ± 3 Ma, respectively (Table 4 and Fig. 14). Because these ages are identical to each other, we interpret them to represent a ca. 44 Ma age of gold mineralization. This is the first reported accurate dating of gold mineralization in this area, and is close to the reported ages (44–59 Ma) of the Maymu gold deposit (Wen et al., 2004; Jiang et al., 2008).

Hou et al. (2006) proposed that the collisional orogen in the Qinghai–Tibet Plateau experienced at least three major orogenic stages. These included syn-collisional orogeny (65–41 Ma), late-collisional transform events (40–26 Ma), and post-collisional extension (25 Ma to the present). Therefore, gold mineralization at Bangbu occurred near the end of the main collisional stage of orogeny.

5.3. Mineralization model

Groves et al. (1998) summarized a series of geological features that define orogenic gold deposits (Table 5). Duoji and Wen (2009), Zhai et al. (2014) and Jiang et al. (2008, 2009) proposed that the Mayum, Zhemulang, Mazhala, and Shalagang Au, Au–Sb, and Sb deposits in southern Tibet belong to the orogenic gold class of deposits (Table 5). The major geological and geochemical features of Bangbu are also quite similar to those of typical orogenic deposits and Mayum (Table 5). Therefore we suggest that the Bangbu deposit is also a large-scale orogenic type gold deposit formed during main collisional stage between the India and Eurasia plates.

Some researchers proposed that collisional orogenic belts, such as Alpine–Himalayan orogen, are detrimental to the preservation of orogenic gold deposits (Groves et al., 1998; Kerrich et al., 2000). This is because they thought that the relatively small scale and shallow vertical fracture systems and the subsequent poor structural interconnectivity of these in the collisional orogens would be not conducive to migration of ore-forming fluids. However, recent studies suggest that orogenic gold deposits are mainly controlled by three factors: (1) abundant andesitic rocks, which have systematically higher Au contents than other rock types; (2) large scale metamorphism from greenschist facies to amphibolite facies within a short period, which releases S^{2-} rich fluids; and (3) fracturing under a compressive/transpressive tectonic regime (Sun et al., 2013). All three conditions are typically present in collisional orogenic belts. For example, earthquakes (Weatherley and Henley, 2013), as well as other changes in a tectonic regime (Sun et al., 2007a, 2007b), may provide favorable conditions for orogenic gold deposit formation in collisional orogenic belts. In addition, detailed field investigation and geochemical studies of orogenic gold deposits in the Qinling orogen by Chen et al. (2008) and Zhou et al. (2014, 2015) suggest that those gold deposits were formed in the tectonic transition from compression to extension during the Jurassic–Early Cretaceous continental collision between the North China and Yangtze cratons, and their genesis can be explained by the so-called "CMF model" (Chen et al., 2004, 2008, 2014; Pirajno, 2009, 2013).

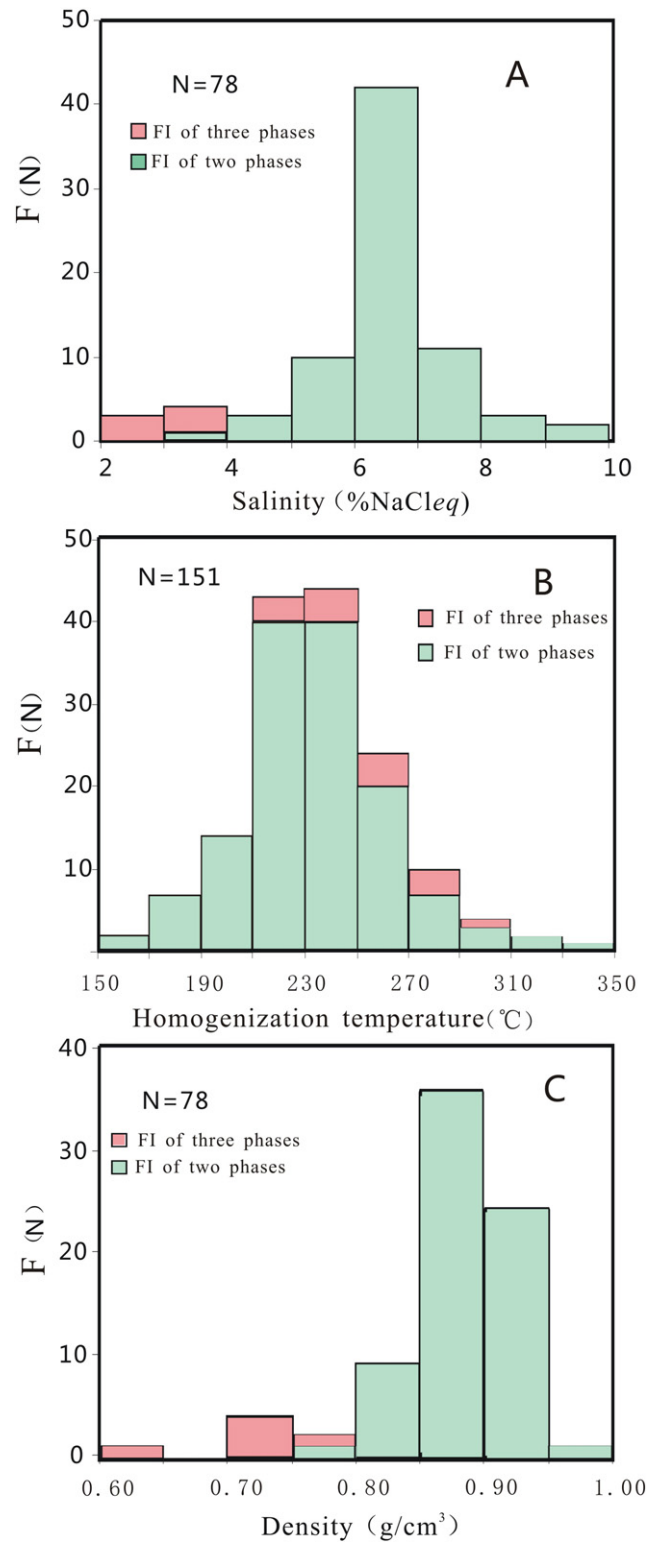

Fig. 10. Histograms of homogenization temperature (Th) (A), salinity (B) and density(C) of CO_2 bearing inclusions in quartz from the Bangbu gold deposit.

Table 2
δD-δ^{18}O-δ^{13}C isotopic compositions of fluid inclusions in auriferous quartz veins from Bangbu gold deposit.

Sample number	Sampling location	Sample name	δD (‰, SMOW)	$\delta^{18}O_Q$ (‰, SMOW)[a]	$\delta^{13}C_{CO2}$ (‰,PDB)	T_h (°C)[b]	$\delta^{18}O_W$ (‰, SMOW)[c]
BB003	III orebody, No.2 adit	Auriferous quartz vein	−64.9	15.0	/	236.1	5.4
BB004			−44.4	18.2	−3.8	235.4	8.5
BB010			−59.4	15.9	/	239.6	6.4
BB013	III orebody, No.4 adit		−49.7	15.6	−2.2	235.4	5.9
BB014	III orebody, second face of No.4 adit	Auriferous quartz sulfide vein	−76.0	15.3	/	250.3	6.4
BB019	III orebody, first face of No.4 adit	Auriferous quartz vein	−61.8	17.7	−5.1	227.9	7.6
BB020	III orebody, third face of No.4 adit	Auriferous quartz sulfide vein	−61.0	16.0	−3.7	235.4	6.3
BB025	III orebody, first face of No.6 adit	Auriferous pyrite quartz vein	−85.2	18.7	/	235.4	9.0
BB027	III orebody, second face of No.6 adit	Auriferous quartz vein	−75.8	15.9	/	229.0	5.9
BB029	III orebody, portal of No.6 adit		−105.3	14.4	/	235.4	4.7
BB032	Unmineralized Upper Triassic metamorphic rocks	Barren quartz vein	−38.2	15.4	−5.1	242.0	6.1

[a] δ^{18}O(‰) of quartz.
[b] Th represents homogenization temperature of fluid inclusions.
[c] δ^{18}O(‰) of fluids calculated based on the measured δ^{18}O of quartz, homogenization temperature of fluid inclusions, and equilibrium oxygen isotope fractionation between quartz and water, $\Delta_{Q\text{-}H2O} = 3.38 \times 10^6/T^2$-3.4 (Clayton et al., 1972).

Table 3
Helium and argon isotope compositions of fluid inclusions in pyrites from Bangbu gold deposit.

Sample number	BB012	BB014	BB015	BB016	BB020	BB025	BB101	BB118	BB017
Sampling location	Portal of No.4 adit	Second face of No.4 adit			Third face of No.4 adit	First face of Bo.6 adit	Sixth ort of No.2 adit	First ort of No.6 adit	Second face of No.4 adit
Description of sample	Pyrite-bearing quartz vein	Galena-pyrite-bearing quartz vein	Sulfide quartz vein	Pyrite-bearing fine-grained quartz vein	Galena-pyrite-bearing quartz vein	Pyrite-bearing quartz vein			Pyrite-bearing carbonaceous sericite phyllite
^{4}He (10^{-8} cm^3 STP/g)	77.4 (52)	47.6 (33)	26.6 (18)	137.5 (93)	43.0 (30)	56.6 (39)	60.1 (41)	54.0 (37)	901.0 (60)
^{40}Ar (10^{-8}cm^3 STP/g)	19.4 (13)	30.5 (21)	12.98 (90)	51.0 (35)	8.01 (54)	93.8 (63)	237.0 (16)	23.6 (16)	20.9 (14)
^{3}He/^{4}He (R_a)	0.385 (11)	1.010 (51)	0.669 (26)	0.174 (12)	0.484 (35)	0.509 (25)	0.802 (28)	0.630 (21)	0.01137 (83)
^{38}Ar/^{36}Ar	0.162 (17)	0.132 (12)	0.172 (12)	0.174 (16)	0.189 (19)	0.167 (21)	0.1818 (39)	0.163 (12)	0.196 (18)
^{40}Ar/^{36}Ar	606.9 (446)	747.9 (163)	1724.9 (1749)	388.3 (126)	689.7 (810)	353.4 (257)	311.9 (66)	1670.3 (277)	1709.7 (1161)
^{40}Ar/^{4}He	0.25	0.64	0.49	0.37	0.19	1.66	3.94	0.44	0.02
Ratio of mantle-derived He (‰)	6.3	16.7	11.0	2.7	7.9	8.3	13.2	10.4	0.0
^{40}Ar* (‰)	51.3	60.5	82.9	23.9	57.2	16.4	5.3	82.3	82.7
^{40}Ar*/^{4}He	0.1286	0.3876	0.4044	0.0886	0.1065	0.2715	0.2073	0.3597	0.0192

The data in the bracket of analytical results are 1σ errors of the last digits.

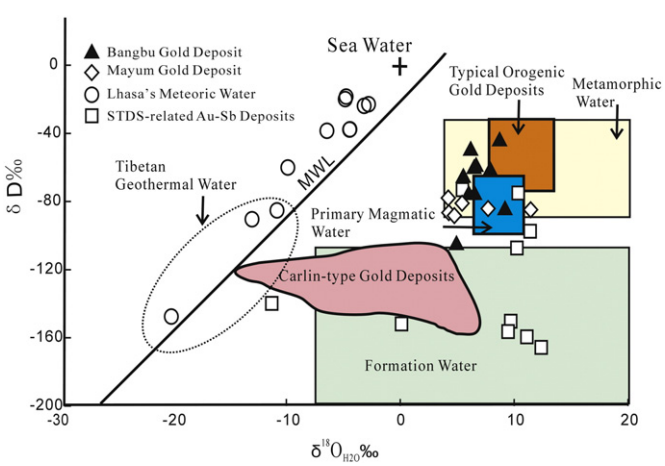

Fig. 11. Plot of δD versus δ^{18}O for ore forming fluids from Bangbu gold deposit. Magmatic, metamorphic, and organic (e.g., devolatilization of organic matter in sediments) after Sheppard (1986); Field for typical orogenic gold deposits after Goldfarb et al. (2004); Field for Nevada Carlin deposits after Field and Fifarek (1985); Field for Daping gold deposit in Ailaoshan gold belt after Sun et al. (2009); Values for geothermal brine in Tibet after Zheng et al. (1982); Values for meteoric water in Lhasa after Zheng et al. (1983); Values for Mayum gold deposit after Wen et al. (2006) and Duoji and Wen (2009); Values for antimony and gold deposits in South Tibet after Yang et al. (2006).

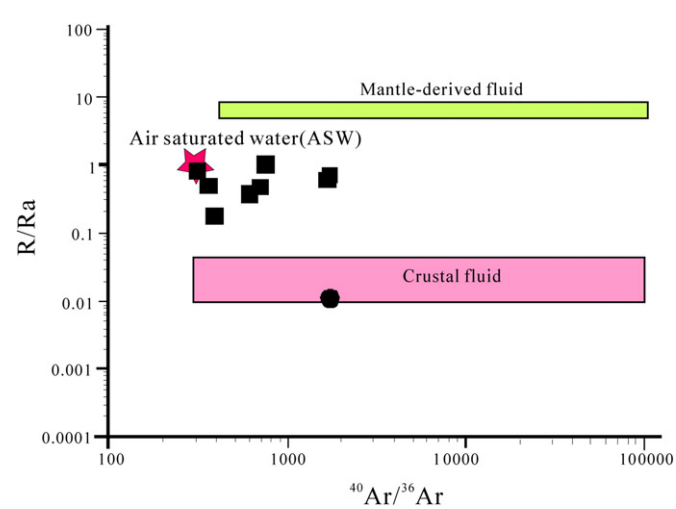

Fig. 12. ^{40}Ar/^{36}Ar vs. R/R_a of the fluid inclusions in pyrites collected from the Bangbu gold deposit (modified after Burnard et al., 1999). Filled squares represent pyrite from quartz veins in Bangbu gold deposit; Filled circles represent pyrite from country rocks of Bangbu gold deposit.

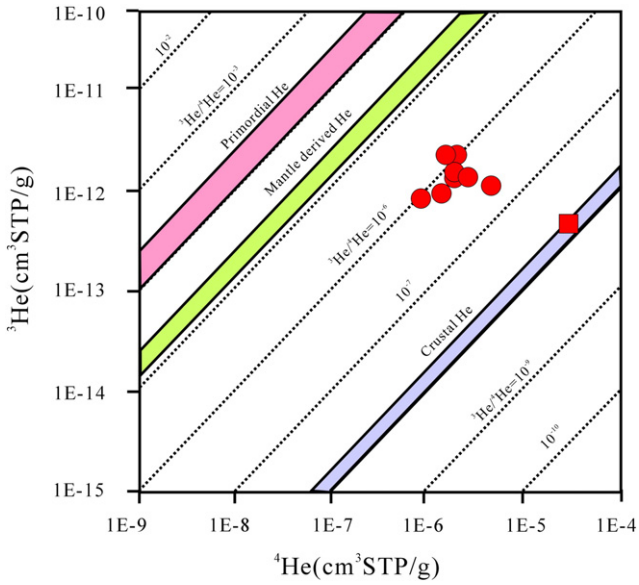

Fig. 13. ^{4}He–^{3}He diagram of the pyrites collected from Bangbu gold deposit (modified after Mamyrin and Tolstikhin, 1984). Filled circles represent pyrite from quartz veins in Bangbu gold deposit; filled squares represent pyrite from country rocks of Bangbu gold deposit.

We found that extensive vertical crust–mantle interaction might have played an important role in the gold mineralization, and thus the ore-forming fluids could contain more mantle-derived components than is typical of many orogenic type gold deposits in the large Cenozoic gold of southwestern China. These deposits occur in a collisional orogenic belt, such as those of the Ailsoahan gold belts along the eastern margin of Qinghai–Tibet Plateau (Sun et al., 2009). Stable and noble gas isotopic analyses described above also demonstrate that a significant mantle component was added to ore-forming fluids at the Bangbu deposit.

During collision between the India and Eurasia plates, large-scale vertical lithospheric shear zones, such as the Qusong–Cuogu–Zhemulang brittle-ductile shear zone and its secondary brittle structures, which host most of the auriferous quartz veins at the Bangbu gold deposit, were formed. The shear zone is a large-scale deep crustal fault, and thus its activity and the subsequent crust–mantle interaction may have triggered the release of large amounts of ore-forming fluids from the deformed and metamorphosed host rocks, the lower crust, and even the upper mantle. At ca. 44 Ma, the middle and lower crust in the Bangbu area suffered high-temperature and high-pressure metamorphism because of ductile deformation and heating by upper mantle magmas. The ore-forming fluids, enriched in CO_2, ^{3}He and probably $Au(HS)_2^-$, and generated by the regional metamorphism and upper mantle magmatic heating, were transported to the middle and upper crust along the ductile shear zone. There they finally precipitated auriferous sulfide–quartz veins in brittle structures because of declining temperature, pressure, and subsequent unmixing. A sketch metallogenic model of the Bangbu gold deposit is presented in Fig. 15.

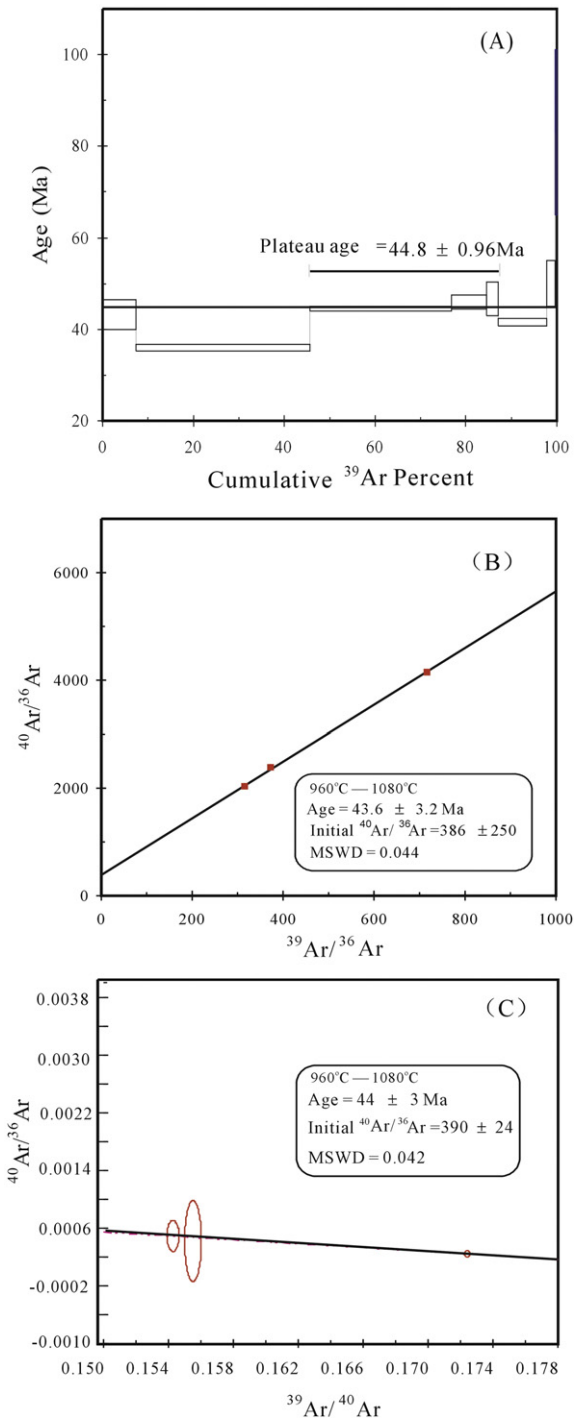

Fig. 14. Apparent ^{40}Ar/^{39}Ar age spectrum (A), normal isochron (B) and inverse isochron (C) of hydrothermal sericites (Sample BB217) from auriferous quartz vein of Bangbu gold deposit.

Table 4
^{40}Ar/^{39}Ar stepwise heating data and apparent ages of muscovite from auriferous quartz vein of Bangbu gold deposit.

T (°C)	$(^{40}Ar/^{39}Ar)_m$	$(^{36}Ar/^{39}Ar)_m$	$(^{37}Ar/^{39}Ar)_m$	$(^{38}Ar/^{39}Ar)_m$	^{40}Ar (%)	$^{40}Ar^*/^{39}Ar$	^{39}Ar ($\times 10^{-14}$ mol)	Fraction of ^{39}Ar released (%)	Age (Ma)	$\pm 1\sigma$ (Ma)
700	1205.9960	3.9427	0.0000	0.7660	3.39	40.9234	0.02	0.31	314	270
800	74.6863	0.2353	0.8456	0.0570	6.97	5.2083	0.47	7.29	43.2	3.3
900	10.8584	0.0221	0.1365	0.0169	39.94	4.3376	2.58	45.75	36.02	0.67
960	5.8047	0.0014	0.0000	0.0128	92.81	5.3874	2.08	76.78	44.63	0.51
1020	6.4860	0.0032	0.0000	0.0125	85.45	5.5426	0.52	84.60	45.9	1.5
1080	6.4347	0.0027	0.0000	0.0121	87.59	5.6361	0.16	87.06	46.7	3.6
1160	5.8793	0.0029	0.1002	0.0129	85.29	5.0151	0.72	97.82	41.58	0.86
1240	12.1370	0.0206	0.0000	0.0153	49.80	6.0447	0.11	99.54	50.0	5.0
1400	80.2161	0.2382	4.0034	0.0731	12.59	10.1280	0.03	100.00	83	18

Table 5
Comparisons of major geological characteristics of Bangbu, Mayum and typical orogenic gold deposits.

Geological features	Bangbu gold deposit	Mayum gold deposit[b]	Typical orogenic gold deposit[a]
Host rocks	Upper Triassic Carbonaceous sercite phyllite and metasandstone	Neoproterozoic–Cambrian schists	Metamorphic rocks
Tectonic background	Located to the south of the east section of the Yarlung Zangbo suture zone in southern Tibet, closely related with the early stage of Indo–Asian continental collision	Located in the western part of the Northern Himalayan tectonic subzone, closely related with the early stage of Indo–Asian collision	Accretionary terranes of convergent plate
Ore-controlling structures	Secondary or third order fractures of Qusong–Cuogu–Zhemulang brittle-ductile shear zone	Shear zone and La'nga Co–Ca Qu anticline near the Yarlung Zangbo suture zone	Secondary to third order brittle structures of large-scale compressed structural zone
Mineral assemblage	Predominantly quartz, with about 5% sulfids	Predominantly quartz, with ≤3%–5% sulfids	Predominantly quartz, with ≤3%–5% sulfids
Hydrothermal alteration	Sulficic, chloritic, carbonate, sericitic and silica, etc.	Sulfidation, sericitization, silicification, carbonatization, and argillation, etc	Carbonatization, sulfidation, chloritization, etc
Compositions of ore-forming fluid	Mainly H_2O–NaCl–CO_2, with a little amount of N_2, CH_4 and other hydrocarbon	CO_2-riching lower salinity NaCl–H_2O ore-forming fluid	CO_2-riching, and CO_2 –H_2O–NaCl ± CH_4 ore-forming fluid
Temperature of ore-forming fluid	190–290 °C	260–280 °C	200–700 °C
Salinity of fluid inclusions	2–9 (% $NaCl_{equiv.}$)	1–6 (% $NaCl_{equiv.}$)	3–10 (% $NaCl_{equiv.}$)

[a] After Groves et al. (1998).
[b] After Duoji and Wen (2009); Jiang et al. (2008, 2009); Huo et al. (2004).

6. Conclusions

1. The Bangbu deposit is a large Cenozoic syn-collisional orogenic gold deposit in Tibet. The second- and third-order brittle fractures adjacent to a large-scale, deep-crustal, brittle-ductile shear zone controlled most of the gold deposition.
2. Fluid inclusion, stable isotope, and noble gas data show that the ore-forming fluid at Bangbu was characterized by high CO_2, medium to lower salinity, and consisted mainly of a metamorphic fluid, with some addition of a mantle-derived fluid. Fluid geochemistry is consistent with that of typical orogenic gold deposits.
3. Dating by $^{40}Ar/^{39}Ar$ shows the gold mineralization occurred near the end of the main collisional event between India and Eurasia. Continental collision between India and Eurasia is defined by the Yarlung Zangbo suture, which is marked by a large-scale vertical lithospheric shear zone. Mantle-derived fluid migrated up the shear zone, mixed with metamorphic fluid and a CO_2-rich fluid developed in the lower crust. The mixed ore-forming fluid then precipitated ores in the brittle structures at ca. 44 Ma.

Acknowledgments

This work was jointly supported by the National Natural Science Foundation of China (No. U1302233, 40830425, 41202055, 40673045, 40873034), the National Key Basic Research Program (No. 2015CB452604, 2009CB421006, 2002CB412610) from the Ministry of Science and Technology, China, the Higher School Specialized Research Fund for the doctoral program funding issue (No. 200805580031), and the Guangdong Province Universities and Colleges Pearl River Scholar Funded Scheme(2011). Dr. Richard Goldfarb of USGS, Dr. Zenqian Hou in the Institute of Geology, CAGS, Professor Franco Pirajno of University of Western Australia, and Professor Yanjing Chen in Beijing University, are appreciated for constructive discussions, suggestions, and polishing the manuscript. We are grateful to Academician Duo Ji, the leader of Tibet Bureau of Geology and Mineral Exploration and Development for his vigorous support during fieldwork. We are also indebted to Liu Hanbin from the Beijing Geological Research Institute of Nuclear Industry for his help with isotopic analyses, and Chen Jian and Zhang Weihong from the Test Center of Sun Yat-sen University for their help with analyses using the Laser Raman. We would like to thank Professor Li Zhaolin for his patient instruction for our fluid inclusion measurements.

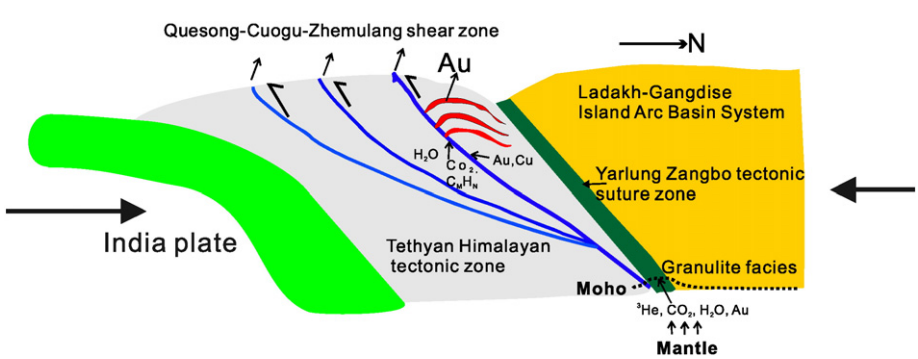

Fig. 15. Schematic map of genetic model of Bangbu gold deposit (Modified after Jiang et al., 2009). At ca. 44 Ma, continental collision between India and Euro–Asia plates between India and Eurasia resulted in formation of Yarlung Zangbo suture zone and the subsequent near-vertical lithospheric shear zones. The mantle-derived fluid was channeled up the shear zone, mixing with metamorphic fluid and a CO_2-rich fluid from the mantle and the lower crust. The mixed fluids migrated into the brittle structures along the shear zone and precipitated auriferous sulfide quartz veins.

References

Aitchison, J.C., Xia, X.P., Baxter, A.T., Ali, J.R., 2011. Detrital zircon U–Pb ages along the Yarlung–Tsangpo suture zone, Tibet: implications for oblique convergence and collision between India and Asia. Gondwana Res. 20, 691–709.

Allégre, C.J., Courtillot, V., Tapponnier, P., 1984. Structure and evolution of the Himalaya-Tibet orogenic belt. Nature 307 (5946), 17–22.

Ballentine, C.J., Burgess, R., Marty, B., 2002. Tracing fluid origin, transport and interaction in the crust. In: Porcelli, et al. (Eds.), Noble Gases in Geochemistry and CosmochemistryReviews in mineralogy & geochemistry vol. 47. Mineralogical Society of America, Washington, pp. 539–614.

Bierlein, F.P., Christie, A.B., Smith, P.K., 2004. A comparison of orogenic gold mineralisation in central Victoria (AUS), western south island (NZ) and Nova Scotia (CAN): implications for variations in the endowment of Palaeozoic metamorphic terrains. Ore Geol. Rev. 25 (1–2), 125–168.

Brown, P.E., 1989. FLINCOR: A microcomputer program for the reduction and investigation of fluid inclusion data. Am. Mineral. 74, 1390–1393.

Burnard, P.G., Hu, R.Z., Turner, G., Bi, X.W., 1999. Mantle, crustal and atmospheric noble gases in Ailaoshan gold deposits, Yunnan Province, China. Geochim. Cosmochim. Acta 63, 1595–1604.

Chen, H.Y., Chen, Y.J., Baker, M.J., 2012a. Evolution of ore-forming fluids in the Sawayaerdun gold deposit in the Southwestern Chinese Tianshan metallogenic belt, Northwest China. J. Asian Earth Sci. 49, 131–144.

Chen, H.Y., Chen, Y.J., Baker, M.J., 2012b. Isotopic geochemistry of the Sawayaerdun orogenic-type gold deposit, Tianshan, northwest China: implications for ore genesis and mineral exploration. Chem. Geol. 310–311, 1–11.

Chen, H.Y., Chen, Y.J., Liu, Y.L., 2001. Metallogenesis of the Ertix gold belt, Xinjiang and its relationship to Central Asia-type orogenesis. Sci. China Earth Sci. 44 (3), 245–255.

Chen, W., Zhang, Y.Q., Jin, G.S., Wang, Q.L., 2006. Late Cenozoic episodic uplifting in southeastern part of the Tibetan plateau—evidence from Ar–Ar thermochronology. Acta Petrol. Sin. 22 (4), 867–872 (in Chinese with English abstract).

Chen, Y.J., Guo, G.J., Li, X., 1998. Metallogenic geodynamic background of gold deposits in granite–greenstone terrains of north China craton. Sci. China Earth Sci. 41 (2), 113–120.

Chen, Y.J., Li, N., Deng, X.H., 2014. Geology and Geochemistry of Molybdenum Deposits in Qinling Orogen. Science Press, Beijing (in Chinese).

Chen, Y.J., Pirajno, F., Qi, J.P., 2008. The Shanggong gold deposit, Eastern Qinling Orogen, China: isotope geochemistry and implications for ore genesis. J. Asian Earth Sci. 33, 252–266.

Chen, Y.J., Pirajno, F., Sui, Y.H., 2004. Isotope geochemistry of the Tieluping silver deposit, Henan, China: a case study of orogenic silver deposits and related tectonic setting. Miner. Deposita 39, 560–575.

Clayton, R.N., Mayeda, T.K., 1963. The use of bromine pentafluoride in the extraction of oxygen from oxide and silicates for isotopic analysis. Geochim. Cosmochim. Acta 27, 43–52.

Clayton, R.N., O'Neil, J.R., Mayeda, T.K., 1972. Oxygen isotope exchange between quartz and water. Geophys. Res. 77, 3057–3067.

Duoji, Wen, C.Q., 2009. Mayum Gold Deposit in Tibet. Geological Publishing House, Beijing, pp. 1–216 (in Chinese).

Field, C.W., Fifarek, R.H., 1985. Light stable-isotopic systematics in the epithermal environment. Rev. Econ. Geol. 2, 99–128.

Geological Survey of Tibet Bureau of Geology and Mineral Exploration and Development. 2006. Prospecting Report of Bangbu Gold Deposit in Jiacha County, Tiber Autonomous Region (Unpublished Research Report, in Chinese).

Goldfarb, R.J., Ayuso, R., Miller, M.L., Ebert, S.W., Marsh, E.E., Petsel, S.A., Miller, L.D., Bradley, D., Johnson, C., Mcclelland, W., 2004. The Late Cretaceous Donlin Creek gold deposit, Southwestern Alaska: controls on epizonal ore formation. Econ. Geol. 99 (4), 643–671.

Goldfarb, R.J., Baker, T., Dube, B., Groves, D.I., Hart, C.J.R., Robert, F., Gosselin, P., 2005. Distribution, character, and genesis of gold deposits in metamorphic terranes. Econ. Geol. 100th Anniversary Volume, 407–450.

Goldfarb, R.J., Groves, D.I., Gardoll, S., 2001. Orogenic gold and geologic time: a global synthesis. Ore Geol. Rev. 18, 1–75.

Groves, D.I., Goldfarb, R.J., Gebre-Mariam, M., Hagemanna, S.G., Robert, F., 1998. Orogenic gold deposits: a proposed classification in the context of their crustal distribution and relationship to other gold deposits types. Ore Geol. Rev. 13, 7–27.

Groves, D.I., Goldfarb, R.J., Robert, F., Hart, C.J.R., 2003. Gold deposits in metamorphic belts: overview of current understanding, outstanding problems, future research, and exploration significance. Econ. Geol. 98, 1–29.

Hou, Z.Q., Yang, Z.M., Qu, X.M., Rui, Z.Y., Meng, X.J., Gao, Y.F., 2009. The Miocene Gangdese porphyry copper belt generated during post-collisional extension in the Tibetan Orogen. Ore Geol. Rev. 36, 25–51.

Hou, Z.Q., Yang, Z.S., Xu, W.Y., Mo, X.X., Lin, L., Gao, Y.F., Dong, F.L., Li, G.M., Qu, X.M., Li, G.M., Zhao, Z.D., Jiang, S.H., Meng, X.J., Li, Z.Q., Qin, K.Z., Yang, Z.M., 2006. Metallogenesis in Tibetan collisional orogenic belt I. mineralization in main collisional orogenic setting. Mineral Deposits 25, 337–358 (in Chinese with English abstract).

Hou, Z.Q., Zhang, H.R., Pan, X.F., Yang, Z.M., 2011. Porphyry Cu (–Mo–Au) deposits related to melting of thickened mafic lower crust: examples from the eastern Tethyan metallogenic domain. Ore Geol. Rev. 39, 21–45.

Hu, R.Z., Bi, X.W., Turner, G., Bi, X.W., 1997. He–Ar isotopic systematics of fluid inclusions in pyrite from Machangqing copper deposit, Yunnan, China. Sci. China. Ser. D Earth Sci. 27 (6), 503–508 (in Chinese).

Huo, Y., Wen, C.Q., Li, B.H., Sun, Y., 2004. Preliminary Study on Geochemical Characteristics of Fluid Inclusions of Mayoum Gold Deposit in Tibet. Contributions to Geology and Mineral Resources Research 19 pp. 100–114 (in Chinese with English abstract).

Jiang, S.H., Nie, F.J., Hu, P., Lai, X.R., 2009. Mayum: an orogenic gold deposit in Tibet, China. Ore Geol. Rev. 36 (1–3), 160–173.

Jiang, S.H., Nie, F.J., Liu, Y.F., 2008. Discussion on genetic type of Mayum gold deposit in Tibet. Mineral Deposits 27 (2), 220–228 (in Chinese with English abstract).

Kerrich, R., Goldfarb, R., Groves, D., Garwin, S., 2000. The characteristics, origins, and geodynamics of supergiant gold metallogenic provinces. Sci. China Ser. D Earth Sci. 43 (S), 1–68.

Li, X.F., Mao, J.W., Chen, W., 2005. $^{40}Ar/^{39}Ar$ dating of sericite from two types of ore and its geological significance in the Miansawa gold deposit, Sichuan. Acta Petrol. Sin. 51 (3), 335–339 (in Chinese with English abstract).

Lu, Y., 2005. Types and basic characteristics of gold deposits in Tibet. Tibet Geol. 2, 42–49 (in Chinese).

Luo, Y.N., Yu, R.L., 2001. Main features and dynamics model of Cenozoic tectonomagmatism in Longmenshan–Jinpingshan intracontinent orogen belt. In: Chen, L.C., Wang, D.H. (Eds.), Study of Himalayan Endogenetic Mineralization. Seismic Publishing House, Beijing, pp. 88–95 (in Chinese).

Lv, Y.P., Yi, J.Z., Xia, B.B., 2005. The geological characteristics of the Bangbu gold deposit in Tibet. Tibet Geol. 2, 21–25 (in Chinese).

Mamyrin, B.A., Tolstikhin, L.N., 1984. Helium Isotope in Nature. Elsevier, Amsterdam.

Mao, J.W., Kerrich, R., Li, H.Y., 2002. High $^{3}He/^{4}He$ ratios in the Wangu gold deposit, Hunan province, China: implications for mantle fluids along the Tanlu deep fault zone. Geochem. J. 36, 197–208.

Mao, J.W., Li, Y.Q., Goldfarb, R., He, Y., Zaw, K., 2003. Fluid inclusion and nobel gas studies of the Dongping gold deposit, Hebei province: a mantle connection for mineralization? Econ. Geol. 98 (3), 517–534.

Moecher, D.P., Valley, W., Essene, E.J., 1994. Extraction and carbon isotope analysis of CO_2 from scapolite in deep crustal granulites and xenoliths. Geochim. Cosmochim. Acta 58 (2), 959–967.

Pan, G.T., Xiao, Q.H., Lu, S.N., Deng, J.F., Feng, Y.M., Zhang, K.X., Zhang, Z.Y., Wang, F.G., Xing, G.F., Hao, G.J., Feng, Y.F., 2009. Subdivision of tectonic units in China. Geol. China 36 (1), 1–28 (in Chinese with English abstract).

Pirajno, F., 2009. Hydrothermal Processes and Mineral System. Springer, Berlin (1250 pp.).

Pirajno, F., 2013. The Geology and Tectonic Settings of China's Mineral Deposits. Springer, Berlin (679 pp.).

Roedder, E., 1984. Fluid inclusions. Reviews in mineralogy. Miner. Soc. Am. 12, 644.

Sheppard, S.M.F., 1986. Characterization and isotopic variations in natural waters. Rev. Mineral. 16, 165–183.

Shi, G.Y., Sun, X.M., Pan, W.J., Hu, B.M., Qu, W.J., Du, A.D., Li, C., 2012. Re–Os dating of auriferous pyrite from the Zhenyuan super-large gold deposit in Ailaoshan gold belt, Yunnan Province, Southwestern China. Chin. Sci. Bull. 57 (35), 4578–4586.

Simmons, S.F., Sawkins, F.J., Schulutter, D.J., 1987. Mantle-derived helium in two Peruvian hydrothermal ore deposits. Nature 329, 429–432.

Stuart, F.M., Burnard, P., Taylor, R.P., Turner, G., 1995. Resolving mantle and crustal contributions to ancient hydrothermal fluid: He–Ar isotopes in fluid inclusions from Dae Hwa W-Mo mineralisation, South Korea. Geochim. Cosmochim. Acta 59, 4663–4673.

Sun, W.D., Ding, X., Hu, Y.H., Li, X.H., 2007a. The golden transformation of the Cretaceous plate subduction in the west Pacific. Earth Planet. Sci. Lett. 262 (3–4), 533–542.

Sun, W.D., Li, S., Yang, X.Y., Ling, M.X., Ding, X., Duan, L.A., Zhan, M.Z., Zhang, H., Fan, W.M., 2013. Large-scale gold mineralization in eastern China induced by an Early Cretaceous clockwise change in Pacific plate motions. Int. Geol. Rev. 55 (3), 311–321.

Sun, X.M., Norman, D.I., Sun, K., Chen, B.H., 1999. N_2–Ar–He systematics and source of ore-forming fluid in Changkeng Au–Ag deposit, Central Guangdong, China. Sci. China Ser. D Earth Sci. 42 (5), 474–481.

Sun, X.M., Wang, M., Xue, T., Ma, M.Y., Li, Y.H., 2004. He–Ar isotopic systematics of fluid inclusions in pyrites from PGE-polymetallic deposits in lower Cambrian black rock series, South China. Acta Geol. Sin. (Engl. Ed.) 78 (2), 471–475.

Sun, X.M., Wei, H.X., Zhai, W., Shi, G.Y., Lian, Y.H., Mo, R.W., Han, M.X., Yi, J.Z., 2010. Ore forming fluid geochemistry and metallogenic mechanism of Bangbu large-scale orogenic gold deposit in southern Tibet, China. Acta Petrol. Sin. 26, 1672–1684 (in Chinese).

Sun, X.M., Xiong, D.X., Shi, G.Y., Wang, S.W., Zhai, W., 2007b. $^{40}Ar/^{39}Ar$ dating of gold deposit hosted in the Daping ductile shear zone in the Ailaoshan gold belt, Yunnan Province, China. Acta Geol. Sin. 81 (1), 88–92 (in Chinese with English abstract).

Sun, X.M., Xiong, D.X., Wang, S.W., Shi, G.Y., Zhai, W., 2006. Noble gases isotopic composition of fluid inclusions in scheelites collected from Daping gold mine, Yunnan province, China, and its metallogenic significance. Acta Petrol. Sin. 22 (3), 725–732 (in Chinese with English abstract).

Sun, X.M., Zhang, Y., Xiong, D.X., Sun, W.D., Shi, G.Y., Zhai, W., Wang, S.W., 2009. Crust and mantle contributions to gold-forming process at the Daping deposit, Ailaoshan gold belt, Yunnan, China. Ore Geol. Rev. 36, 235–249.

Wang, D.H., Yang, J.M., Xue, C.J., 2001. Geochronological Evidences of Himalayan Gold Deposits in Jinshajiang–Lancangjiang–Nujiang–Daduhe Region, Southwestern China. Study of Himalayan Endogenetic MineralizationSeismic Publishing House, Beijing, pp. 88–95 (in Chinese).

Wang, F., He, H.Y., Zhu, R.X., Sang, H.Q., Wang, Y.L., Yang, L.K., 2006. Intercalibration of international and domestic $^{40}Ar/^{39}Ar$ dating standards. Sci. China. Ser. D Earth Sci. 49 (5), 461–470.

Weatherley, D.K., Henley, R.W., 2013. Flash vaporization during earthquakes evidenced by gold deposits. Nat. Geosci. 6 (4), 294–298.

Wei, H.X., Sun, X.M., Zhai, W., Shi, G.Y., Liang, Y.H., Mo, R.W., Han, M.X., Yi, J.Z., 2010. He–Ar-S isotopic compositions of ore-forming fluids in the Bangbu large-scale gold deposit in southern Tibet, China. Acta Petrol. Sin. 26, 1685–1691 (in Chinese).

Wen, C.Q., Duoji, Fan, X.P., Hu, X.C., Li, B.H., Sun, Y., Liu, W.Z., Huo, Y., Wen, Q., Ren, W.J., 2006. Characteristics of ore fluids of the Mayum gold deposit, western Tibet, China. Reg. Geol. China 25 (1–2), 261–266 (in Chinese with English abstract).

Wen, C.Q., Duoji, S.Y., Fan, X.P., Xu, L., Huo, Y., Geshan, D.Q., Luo, X.J., 2004. ^{40}Ar–^{39}Ar dating of quartz from gold-bearing quartz veins in the Mayum gold deposit, Burang, Tibet, and its geological significance. Geol. Bull. China 23, 686–688 (in Chinese with English abstract).

Winckler, G., Aeschbach-Hertig, W., Kipfer, et al., 2001. Constraints on origin and evolution of Red brines from helium and argon isotopes. Earth Planet Sci Lett. 184, 671–683.

Xiong, D.X., Sun, X.M., Shi, G.Y., 2007a. Geochemistry and metallogenic model of Ailaoshan cenozoic orogenic gold belt in Yunnan province, China. Geological Publishing House, Beijing, pp. 1–144 (in Chinese with English abstract).

Xiong, D.X., Sun, X.M., Zhai, W., Shi, G.Y., Wang, S.W., 2007b. CO_2-rich fluid inclusions in auriferous quartz veins from the Daping ductile shear zone hosted gold deposit in Yunnan province, China, and its implications for gold mineralization. Acta Geol. Sin. 81 (5), 640–653 (in Chinese with English abstract).

Xu, Y.C., Shen, P., Tao, M.X., Liu, W.H., 1996. Geochemistry on mantle-derived volatiles in natural gases from eastern China oil/gas provinces (I) — a novel helium resource-commercial accumulation of mantle-derived helium in the sedimentary crust. Sci. China. Ser. D Earth Sci. 26 (1), 1–8 (in Chinese).

Xue, C.J., Chen, Y.C., Wang, D.H., Yang, J.M., Yang, W.G., Zeng, R., 2003. The Jinding and Baiyangping deposits, Westnorthern Yunnan: geological feature, He, Ne and Xe isotope compositions, and metallogenic epoch. Sci. China. Ser. D Earth Sci. 33 (4), 315–322 (in Chinese).

Yan, S.H., Yang, J.M., Wang, D.H., Chen, Y.C., Xu, J., 2002. $^{40}Ar/^{39}Ar$ dating of the Daduhe gold orefield in Kangding, Sichuan — new evidence of the Himalayan Mineralization and its implications. Acta Geol. Sin. 76 (3), 384–388 (in Chinese with English abstract).

Yang, Z.S., Hou, Z.Q., Gao, W., Wang, H.P., Li, Z.Q., Meng, X.J., Qu, X.M., 2006. Metallogenic characteristics and genetic model of antimony and gold deposits in south Tibetan detachment system. Acta Geol. Sin. 80, 1377–1391 (in Chinese with English abstract).

Ye, X.R., Wu, M.B., Sun, M.L., 2001. Determination of the noble gas isotopic composition in rocks and minerals by mass spectrometry. Rock Miner. Anal. 20 (3), 174–178 (in Chinese with English abstract).

Zeng, Z.G., Qin, Y.S., Zhai, S.K., 2001. He, Ne and Ar isotope compositions of fluid inclusions in hydrothermal sulfides from the TAG hydrothermal field, Mid-Atlantic Ridge. Sci. China D 44 (3), 221–228.

Zhai, W., Sun, X.M., Yi, J.Z., Zhang, X.G., Mo, R.W., Zhou, F., Wei, H.X., Zeng, Q.G., 2014. Geology, geochemistry, and genesis of orogenic gold–antimony mineralization in the Himalayan orogen, South Tibet, China. Ore Geol. Rev. 58 (1), 68–90.

Zhao, K.D., Jiang, S.Y., Xiao, H.Q., Xiao, H.Q., Ni, P., 2002. Origin of ore-forming fluidof the Dachang Sn-polymetallic ore deposit: evidence from helium isotopes. Chin. Sci. Bull. 47 (12), 1041–1045.

Zheng, S.H., Hou, F.G., Ni, B.L., 1983. Study of H–O isotope of meteoric water in China. Chin. Sci. Bull. 13, 801–806 (in Chinese).

Zheng, S.H., Zhang, Z.F., Ni, B.L., Hou, F.G., Shen, M.Z., 1982. Study of H–O isotope of geothermal water in Tibet. Acta Sci. Nat. Univ. Pekin. 1, 99–106 (in Chinese).

Zheng, Y.F., Chen, J.F., 2000. Stable Isotope Geochemistry. Science Press, Beijing, pp. 1–275 (in Chinese).

Zhou, Z.J., Chen, Y.J., Jiang, S.Y., Hu, C.J., Qin, Y., Zhao, H.X., 2015. Isotope and fluid inclusion geochemistry and genesis of the Qiangma gold deposit, Xiaoqinling gold field, Qinling Orogen, China. Ore Geol. Rev. 66, 47–64.

Zhou, Z.J., Chen, Y.J., Jiang, S.Y., Zhao, H.X., Qin, Y., Hu, C.J., 2014. Geology, geochemistry and ore genesis of the Wenyu gold deposit, Xiaoqinling gold field, Qinling Orogen, southern margin of North China Craton. Ore Geol. Rev. 59, 1–20.

Zhu, D.C., Zhao, Z.D., Niu, Y.L., Dilek, Y., Hou, Z.Q., Mo, X.X., 2013. The origin and pre-Cenozoic evolution of the Tibetan Plateau. Gondwana Res. 23, 1429–1454.